A stable and less grid-size dependent high-resolution scheme for kinematic wave open channel routing for large-scale watershed modeling in British Columbia, Canada

Charles Luo, BC River Forecast Centre, February 2021.

Note: *This technical report was recompiled from a manuscript that was submitted to the Journal of Hydrology for publication in June 2016. The journal rejected the manuscript after a major revision. However, considering that the manuscript includes a lot of detailed information of the advanced science included in the CLEVER Mode, for which the author had invested a significant amount of time in gathering and reading references, collecting and treating data, carrying out a series of scientific researches, and compiling the results and findings into a manuscript, the author decided to convert the manuscript into a technical report for reference of the River Forecast Centre staff and other researchers who are interested.*

Abstract: The objective of this study is to find or develop an appropriate and efficient numerical scheme for the kinematic wave open channel routing for the large-scale watersheds in British Columbia, Canada, which include a number of regulated rivers. This paper starts with examination of four commonly used numerical schemes, the Chow Linear and Nonlinear, HEC and KINEROS schemes with a hypothetical inflow and then three typical observed hydrographs from British Columbia. In order to overcome the difficulties faced by the four commonly used schemes in routing the regulated hydrograph observed in the Peace River, a high-resolution scheme is developed. The scheme developed in this study employs a method similar to the SIMPLE to solve the finite difference equation iteratively. The high-resolution scheme includes the Minmod flux limiter and therefore is stable or oscillation free. It is also found less grid-size dependent with respect to numerical dispersion and diffusion. Therefore, the scheme allows a modeller to select more flexibly the sizes of the spatial and temporal increments and is more appropriate and efficient for the kinematic wave open channel routing for the large-scale watersheds in British Columbia.

Keywords: Kinematic wave, high resolution scheme, total variation diminishing, distributed open channel routing.

Citing this document:

Luo, C., 2021. A stable and less grid-size dependent high-resolution scheme for kinematic wave open channel routing for large-scale watershed modeling in British Columbia, Canada. Technical Report. BC River Forecast Centre.

Contents

1. Introduction

British Columbia (BC) is the Pacific coastal province of Canada, in which there are seven major watersheds with a total area of 726,986 km^2 or 77% of the province's total land area. BC's watersheds are characterized by their special geographic locations (high latitudes and close to the Pacific coast) and their large scales. From the hydrological perspective, BC's watersheds are mountainous and subject to both snowmelt and coastal storm flooding. Besides, a number of rivers in BC's watersheds are regulated and the regulated stream systems pose extra complications to the channel routing. The characteristics of BC's watersheds and the great heterogeneity or variability issues related to the large scales of BC's watersheds are described in detail in Luo et al. (2015) and Luo (2015). A hybrid large-scale watershed model, the Channel Link Evolution Efficient Routing Model (the CLEVER Model) (Luo, 2015; Luo et al., 2015), which consists of a lumped watershed routing sub-model and a distributed open channel routing sub-model, was developed for the purpose of operational real-time flood forecast in BC. As a watershed model for BC, it must be able to address the special requirements stemmed from the great heterogeneity of BC's large-scale watersheds. In the meantime, as an operational real-time flood forecast model, it also must be very time efficient. Based on these considerations, a lumped watershed routing sub-model and a distributed open channel routing sub-model using the kinematic wave are incorporated in the CLEVER Model. The model structure and the hydrological cycle including precipitation, evapotranspiration, infiltration, snow melting, the overland surface flow, etc. are included in the lumped watershed routing sub-model which was described in detail in Luo (2015). This paper is only focused on the development of the methodology for the distributed open channel routing sub-model using the kinematic wave.

One advantage of the kinematic wave routing is that it can be developed with little or no streamflow data (Dawdy, 1990). Because of this and the simplicity, the kinematic wave routing is popular in open channel routing and watershed modeling. The following is a list of examples of hydrologic models using the kinematic wave for open channel routing from the 1990s to the recent years: the Hydrologic Ensemble Forecast Service (HEFS) of the National Oceanic and Atmospheric Administration (NOAA) National Weather Service (NWS) (Demargne et al, 2014), which is part of the Advanced Hydrologic Prediction Service (AHPS) (McEnery et al., 2005), AHPS's improved operational foundation - the National Weather Service River Forecast System (NWSRFS) – the HL-RMS (Koren et al., 2004), the EFAS (Thielen et al., 2009), GloFAS (Alfieri et al., 2013) and AFFS (Thiemig at el., 2015), which were based on the LISFLOOD (Burek et al., 2013; de Roo, 1999), Ye et al. (2013), Lee and Huang (2012), Syed at al. (2012), HEC-HMS (US Army Corps of Engineers, 2000) and HEC-1 (US Army Corps of Engineers, 1993), and KINEROS (Smith et al., 1995; 2012). In this study, it is difficult to obtain detail streamflow data for all the rivers in BC's large-scale watersheds. Meanwhile, the application of this study is an operational real-time flood forecasting model and the requirement of time efficiency (producing

forecasts for the entire province in a very short time, e.g. 2 to 4 hours) does not allow the use of a very complicated model. Therefore, the kinematic wave is selected for the distributed open channel routing in this study.

In watershed modeling, the kinematic wave approximation is a common treatment to the Saint Venant Equations when the inertia and pressure forces are not important. Moramarco and Singh (2000) concluded that both the inertia and pressure forces can be neglected for many steady uniform flow conditions if the channel slope is greater than 1%. After comparing the hydrographs from the numerical solutions of the kinematic wave and dynamic wave, Lee and Huang (2012) concluded that the deviation of the hydrographs from the two numerical solutions is small if the channel slope is larger than 0.001. Actually, Ponce (1996) have defined a broadened criterion for the applicability of the kinematic wave and stated that the kinematic wave is applicable for a wide range of field situations, both "short" mountain streams and "long" alluvial rivers, both steep and mild basins and both fast-rising and slow-rising hydrographs, providing that the product of the time to peak (or time of rise) and the riverbed slop is significant large.

Besides the channel slope and wave patterns which may affect the accuracy of the kinematic wave routing, researchers have also noticed that numerical solutions of the kinematic wave are strongly dependent on the sizes of spatial and temporal increments. Hromadka and DeVries (1988) had examined the computation error of the kinematic wave routing due to numerical diffusion and the selection of the modeling reach length and the size of the time increment, and therefore they recommended that use of the kinematic wave method for channel routing in watershed models should be reconsidered. Ponce (1991) concluded that kinematic wave solutions using finite differences possess intrinsic numerical diffusion and dispersion which means that the solutions are a function of the gird size. However, some other researchers argued for the contrary, e.g., Goodrich (1992) pointed out that, under certain conditions, calibration for a suitable and statistically interpreted roughness coefficient value that replicates watershed behavior can proceed with the kinematic wave routing.

Yu and Duan (2014) have evaluated four high resolution schemes for the kinematic wave overland flow routing on a miniature/experimental scale. This study focuses on the numerical schemes and developing a different numerical scheme for the kinematic waver open channel routing for the large-scale watersheds in BC. In the coming sections, three typical hydrographs from BC's large-scale watersheds are first presented, and then the four commonly used numerical schemes for the kinematic wave open channel routing, the linear and nonlinear schemes by Chow at al. (1988), the HEC scheme including HEC-1 (US Army Corps of Engineers, 1993) and HEC-HMS (US Army Corps of Engineers, 2000), and the KINEROS scheme (Smith et al., 1995, 2012), are described and examined with the slightly modified example by Chow at al. (1988) and the three typical observed hydrographs recorded in BC's watersheds. After that, a new high resolution numerical scheme for the kinematic wave open channel routing is developed and then examined with the regulated hydrograph observed in the Peace River. In

order to confirm the stability of the scheme, a hypothetical, rectangular hydrograph is utilized to further examine the scheme. And finally, the performance of the scheme is compared with that of the Muskingum-Cunge (MC) approach.

2. BC's watersheds and categories of hydrographs

Most BC's watersheds are of very large scales, e.g., the Fraser River has a drainage area of 232,136 km^2 and a total of river length of 11,200 km. Most of these watersheds are snow-dominated watersheds, in which the majority of floods are freshet season snowmelt floods that have a relatively longer rising time or time to peak. In addition to the snowmelt floods, some of the Pacific coastal watersheds also suffer from coastal storm flash floods that have a much shorter rising time. In the meantime, some river systems in BC are regulated and the flows are human controlled through operations of the upstream gates, dam spillways or other hydraulic structures and the hydrographs are unnatural and sometimes even very odd. A full description of the characteristics of BC's watersheds is given by Luo (2015).

Fig. 1 shows three observed hydrographs from three hydrometric stations of the Water Survey of Canada (WSC) located in BC's watersheds. Fig. 1 (a) shows the hydrograph of a snowmelt flood from March 7, 2015 to April 20, 2015 recorded at the WSC station Fraser River near Marguerite (08MC018). The hourly average flow is calculated from the observation data in a 5 minute interval. For this hydrograph, the rising time of the major peak is 96 hours or 4 days. Fig. 1 (b) shows the hydrograph of a coastal storm flood from October 13, 2003 to October 28, 2003 recorded at the WSC station Lillooet River near Pemberton (08MG005). The hourly flow is distributed from the daily data. For this hydrograph, the rising time is 36 hours or 1.5 days. Fig.1 (c) shows the hydrograph for a five day period from February 12, 2016 to February 16, 2016 recorded at the WSC station Peace River at Hudson Hope (07EF001), which is a regulated station, and from which 8.5 km upstream is the Peace Canyon Dam that controls the downstream flow of the Peace River. The hourly average flow is calculated from the observation data in a 5 minute interval. For this rare human control hydrograph, the rising time of the first rise after the first plunge is only 4 hours. The above three categories of hydrographs are characterized by their different rising times. The rising time of a snowmelt flood is usually much longer than that of a coastal storm flood, while the rising time of a regulated hydrograph is random and in the example given in Fig. 1 (c), the rising time is much shorter than those of the natural hydrographs.

(a)

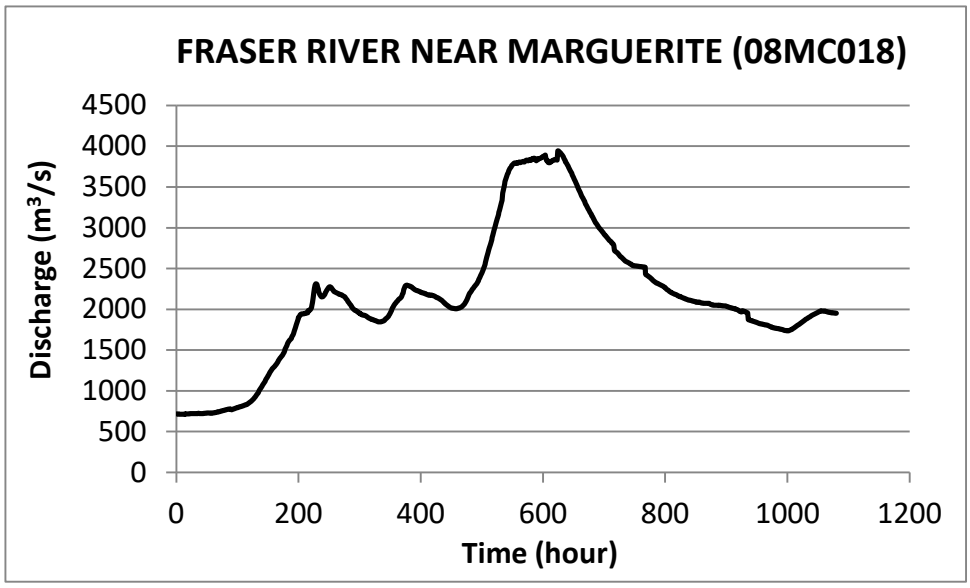

(b)

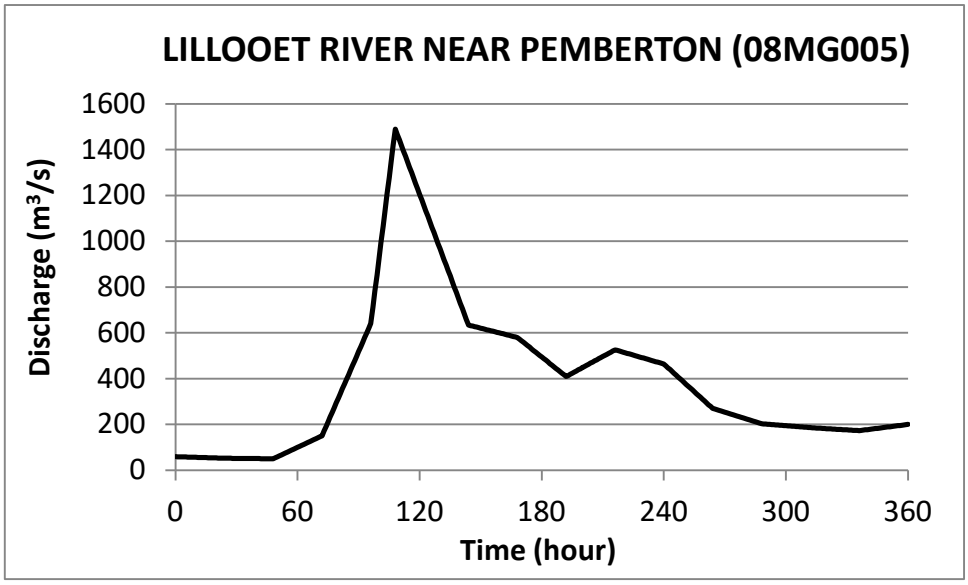

Figure 1. Three observed hydrographs in BC's large-scale watersheds: (a) a snowmelt flood hydrograph recorded at station Fraser River near Marguerite (08MC018), (b) a coastal storm flood hydrograph recorded at station Lillooet River near Pemberton (08MG005), (c) a regulated hydrograph recorded at station Peace River at Hudson Hope (07EF001). (Continued next page.)

(c)

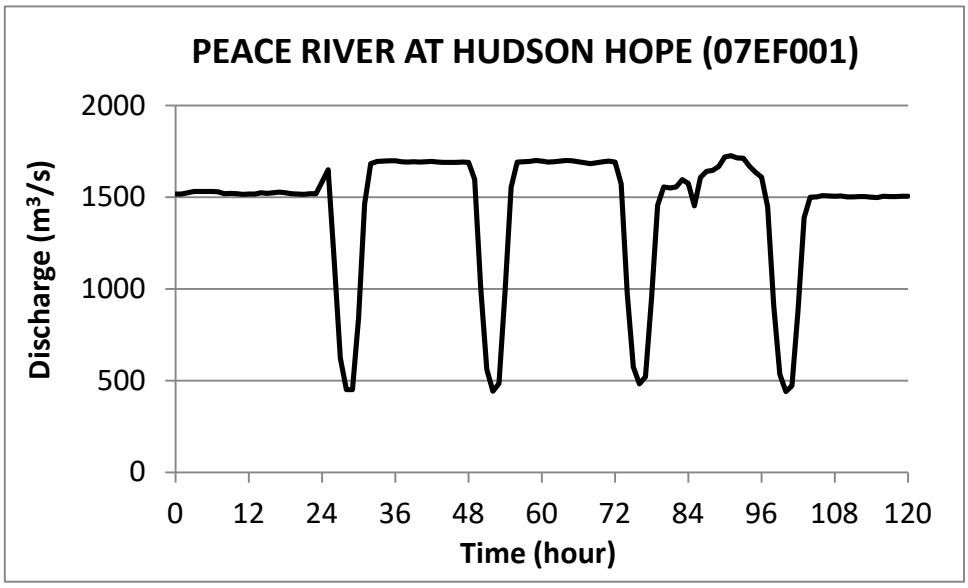

Figure 1. Three observed hydrographs in BC's large-scale watersheds: (a) a snowmelt flood hydrograph recorded at station Fraser River near Marguerite (08MC018), (b) a coastal storm flood hydrograph recorded at station Lillooet River near Pemberton (08MG005), (c) a regulated hydrograph recorded at station Peace River at Hudson Hope (07EF001).

3. Four commonly used numerical schemes for kinematic wave open channel routing

3.1 Description of the four schemes and examination with a hypothetical hydrograph

Chow et al. (1988) presented two numerical schemes, the linear scheme (hereinafter referred to as the Chow Linear scheme) and the nonlinear scheme (hereinafter referred to as the Chow Nonlinear scheme). The latter (nonlinear scheme) has been largely used in watershed modeling, e.g. the HL-RMS (Koren et al., 2004) family and the LISFLOOD (Burek et al., 2013; de Roo, 1999) family, and the former (linear scheme) is also used by modellers such as Lee and Huang (2012). It is found that the Chow Nonlinear scheme is unconditionally stable (Koren et al., 2004; Singh, 1996), and after extensive tests with a wide range of sizes of spatial and temporal increments by the author of this study, it is found that the Chow Linear scheme is also unconditional stable. The other commonly used first order scheme is the HEC including HEC-1 (US Army Corps of Engineers, 1993) and Hydrologic Modeling System (HEC-HMS) (US Army Corps of Engineers, 2000). The HEC scheme is deliberately designed to avoid the unstable issue by switching between the "standard form" and "conservation form." In the HEC model, the "standard form" is used when the stability factor is less than 1 or the kinematic wave celerity (c_k) is smaller than the quotient of spatial increment and the temporal increment (Δx/Δt) and the "conservation form" is used otherwise. In the meantime, the Kinematic Simulation of Catchment Runoff and Erosion Processes (KINEROS) (Smith et al., 1995; 2012), which was developed in the Southwest Watershed Research

Center of the United States Department of Agriculture, is another commonly used scheme for the kinematic wave open channel routing. The KINEROS scheme is actually a second order scheme which is intrinsically unstable for certain types of hydrographs and sizes of spatial and temporal increments even though a weighting factor (θ=0.6 to 0.8) is introduced to the space derivative (only). Equations of the above four schemes are available from easily accessible references and therefore are omitted here for conciseness of this paper.

The Muskingum-Cunge (MC) approach is also a commonly used method for the open channel routing in the hydrologic community. However, because of its lack of mass balance and inconsistency of the water volume stored in the channel, MC is not a kinematic wave in a strict sense and thus not considered from the beginning in this study. Discussion of MC is beyond the scope of this paper and can be found in Todini (2007). However, at the end of Section 4, MC is utilized to simulate the regulated inflow for the purpose of comparison with the scheme developed in this study.

The slightly modified version of Example 9.6.1 of Chow et al. (1988) on page 297 is first employed to examine the magnitude of numerical dispersion and attenuation of the above four schemes. The modification is only doubling the channel length from 4.572 km (15,000 ft) to 9.144 km (30,000 ft) in order to obtain an extra scenario of larger sizes of spatial and temporal increments. And all United States customary units used in the example are converted into the SI units as well. This example consists of an inflow of a triangular wave and a rectangular channel with the following parameters: width (b) = 60.96 m (200 ft), slope (S_0) = 0.01, and Manning's roughness coefficient (n) = 0.035. There is no lateral inflow and the initial condition is a uniform discharge of 56.634 m^3/s (2000 cfs).

Fig. 2 shows the hydrographs of model outputs from the four schemes at the outlet of the 9.144 km long channel. The figure shows the hydrographs for three scenarios comparing with the analytical solution which is obtained by using the method by Chow et al. (1988). The three scenarios are [Δx = 0.305 km (1000 ft), Δt = 1 minute], [Δx = 0.914 km (3000 ft), Δt = 3 minute] and [Δx = 3.05 km (10000 ft), Δt = 10 minute]. For all the three scenarios, Δx/Δt = 5.08 m/s, which is slightly greater than the maximum kinematic wave celerity (4.6 m/s).

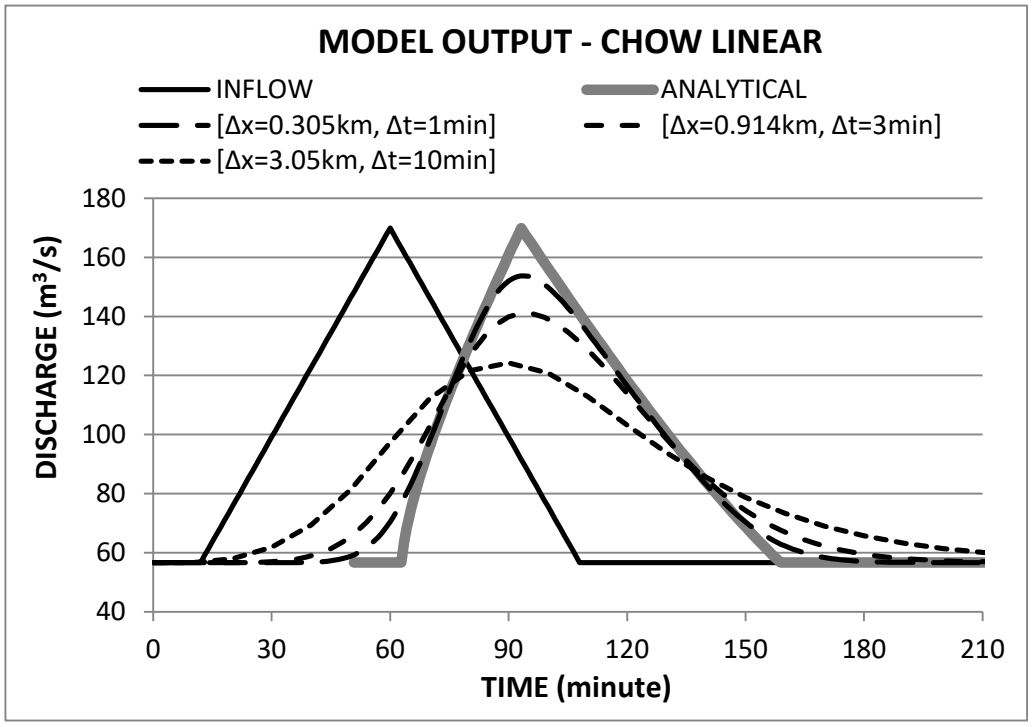

(a)

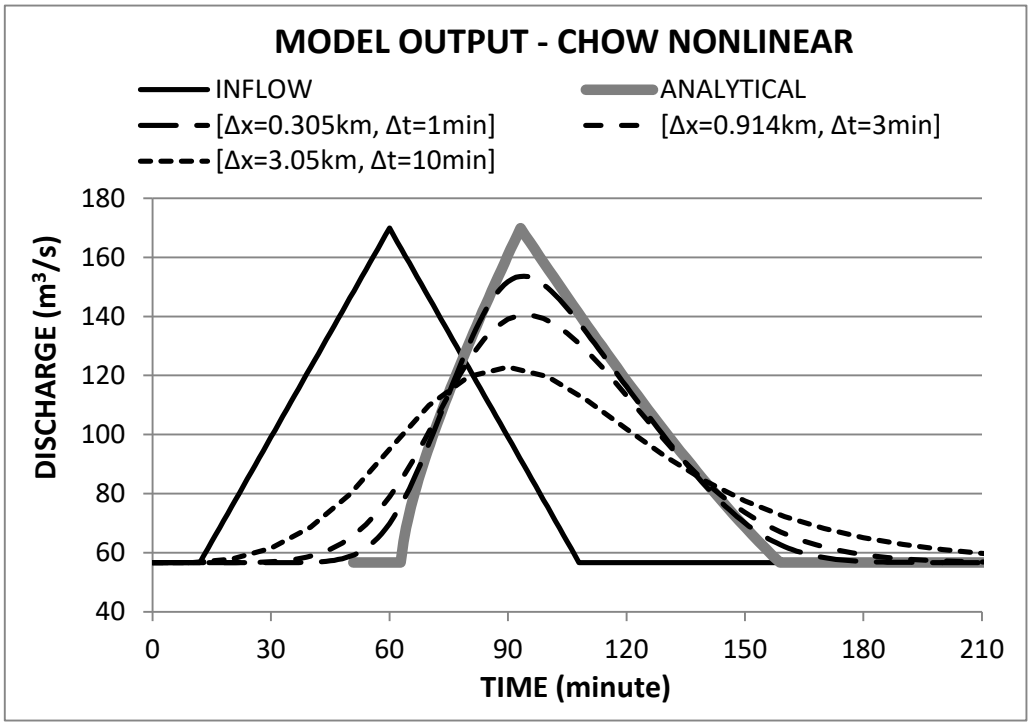

(b)

Figure 2. Comparison of output hydrographs for three scenarios ([Δ x= 0.305 km, Δt = 1 minute], [Δx = 0.914 km, Δt = 3 minute] and [Δx = 3.05 km, Δt = 10 minute]) from Chow Linear, Chow Nonlinear, HEC, and KINEROS (θ=0.6 and 0.8) schemes with the analytical solution: (a) Chow Linear, (b) Chow Nonlinear, (c) HEK, (d) KINEROS (θ=0.6), and (e) KINEROS (θ=0.8). (Continued next pages.)

(c)

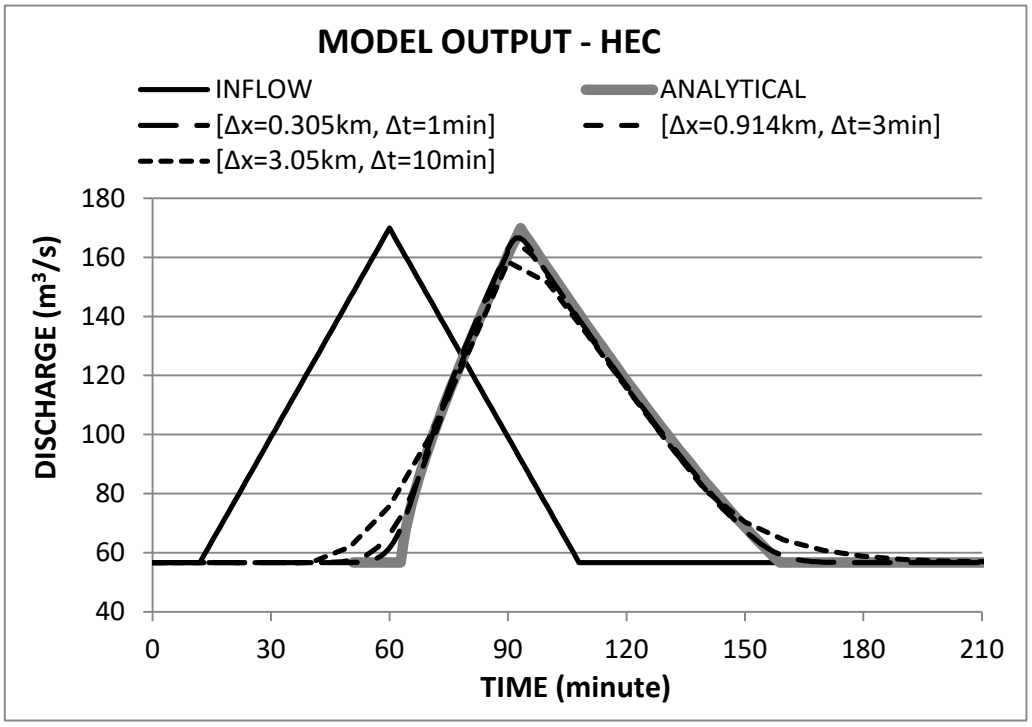

(d)

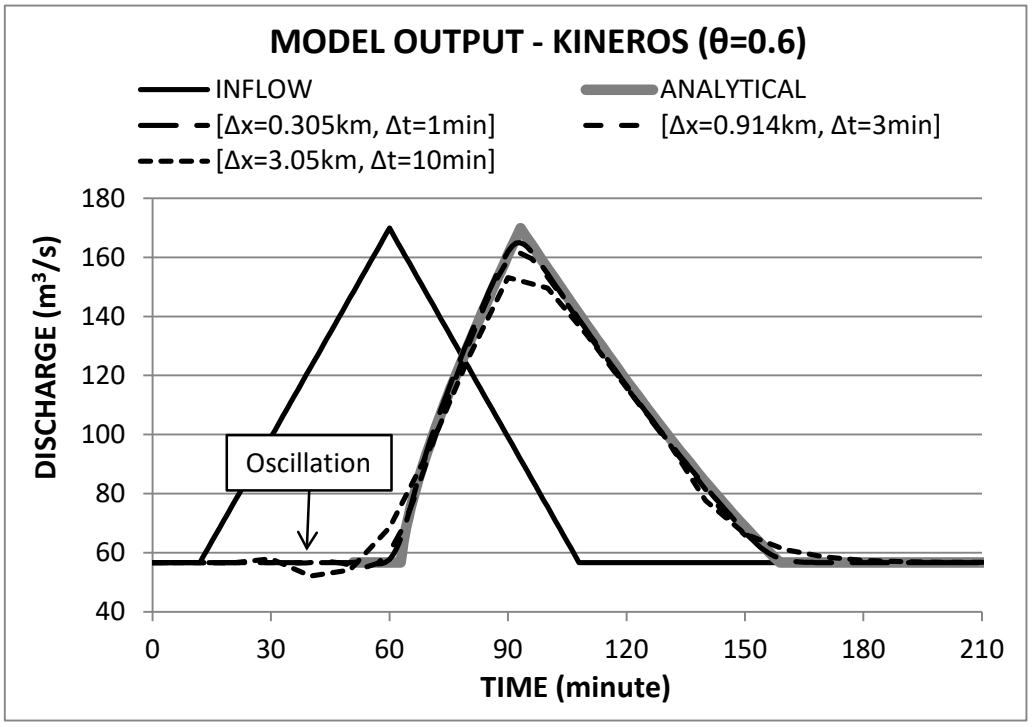

Figure 2. Comparison of output hydrographs for three scenarios ([Δ x= 0.305 km, Δt = 1 minute], [Δx = 0.914 km, Δt = 3 minute] and [Δx = 3.05 km, Δt = 10 minute]) from Chow Linear, Chow Nonlinear, HEC, and KINEROS (θ=0.6 and 0.8) schemes with the analytical solution: (a) Chow Linear, (b) Chow Nonlinear, (c) HEK, (d) KINEROS (θ=0.6), and (e) KINEROS (θ=0.8). (Continued next page.)

(e)

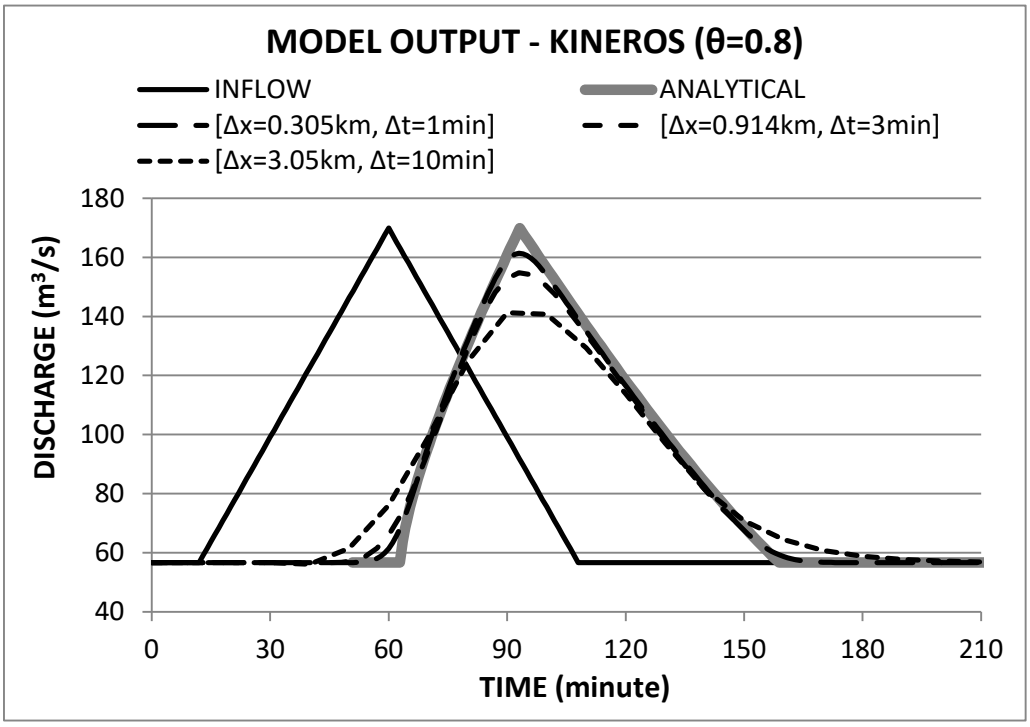

Figure 2. Comparison of output hydrographs for three scenarios ([Δ x= 0.305 km, Δt = 1 minute], [Δx = 0.914 km, Δt = 3 minute] and [Δx = 3.05 km, Δt = 10 minute]) from Chow Linear, Chow Nonlinear, HEC, and KINEROS (θ=0.6 and 0.8) schemes with the analytical solution: (a) Chow Linear, (b) Chow Nonlinear, (c) HEK, (d) KINEROS (θ=0.6), and (e) KINEROS (θ=0.8).

At least three phenomena can be seen from Fig. 2. First, all the four schemes demonstrate a certain degree of numerical dispersion and attenuation and the magnitudes of numerical dispersion and attenuation are different for different schemes. The Chow Nonlinear scheme has the greatest numerical dispersion and attenuation while the HEC scheme has the smallest. The magnitude of numerical dispersion and attenuation of the Chow Linear scheme is only slightly smaller than that of the Chow Nonlinear scheme but both are much more prominent than those of the other two schemes, the HEC and KINEROS. The KINEROS scheme is in between the Chow Linear/Nonlinear schemes and the HEC scheme with respect to the numerical dispersion and attenuation and the larger the θ, the more prominent the numerical dispersion and attenuation. Second, all schemes show increasing magnitudes of numerical dispersion and attenuation when the size of the spatial increment increases proportionally with that of the temporal increment while the ratio of Δx/Δt remains unchanged. This method to increase spatial and temporal increments is found in Chow et al. (1988). The increase of the magnitude of numerical dispersion and attenuation with the proportional increasing of Δx and Δt for the Chow Linear and Nonlinear schemes is the greatest among the four schemes and that for the HEC scheme is the smallest, with that for the KINEROS scheme in between. Third, oscillation is present before the rise

of the hydrograph for the KINEROS scheme (more obvious for θ=0.6) while the Chow Linear/Nonlinear and HEC schemes are oscillation free.

3.2. Routing observed natural inflows and comparing outflows from the four schemes

In this subsection, the four numerical schemes are employed to route two observed inflows, which are the first two observed hydrographs shown in Fig. 1 (a) and (b). The outflows from the model outputs of the four numerical schemes are compared among themselves, without comparing with observed hydrographs because the lateral inflows from tributaries and the local drainage area are not taken into account for simplicity and/or no observation data is available.

The slow rising (and slow dropping) hydrograph of snowmelt flood recorded at the WSC station Fraser River near Marguerite (08MC018) shown in Fig. 1 (a) is the first observed hydrograph that is used to examine the performances of the four numerical schemes. About 400 km downstream is another WSC station, Fraser River at Hope (08MF005), and the four schemes are used to route the inflow hydrograph downstream for a distance of 400 km and the output hydrographs are compared at the location of this WSC station. For simplicity, the lateral inflows from the tributaries and the local drainage area are not taken into account. The river is assumed rectangular with the following parameters: width (b) = 100 m, slope (S0) = 0.001, and Manning's roughness coefficient (n) =0.057. Considering the river length (400 km) and the minimum and maximum kinematic wave celerities (2.388 m/s and 4.194 m/s respectively) of the inflow hydrograph, the following two scenarios are designed for the examination, Scenario 1: [Δx = 10 km / Δt = 1 h] (Δx/Δt = 2.778 m/s) and Scenario 2: [Δx = 20 km / Δt = 1 h] (Δx/Δt = 5.556 m/s). Fig. 3 shows the comparison of the output hydrographs from the four schemes, and (a) and (b) for Scenario 1 and (c) and (d) for Scenario 2. One can see from Fig. 3 that the deviations of the output hydrographs from the four schemes for both scenarios are very small and the output hydrographs are almost identical. The maximum deviations of the peak are 1.5 % for Scenario 1 (between Chow Nonlinear and KINEROS) and 2.8 % for Scenario 2 (between Chow Nonlinear and HEC), respectively. This means that all the four schemes perform very closely for simulation of the slow rising (and slow dropping) snowmelt flood hydrographs.

The coastal storm flood hydrograph recorded at the WSC station Lillooet River near Pemberton (08MG005) shown in Fig. 1 (b) is the second observed hydrograph that is utilized to examine the performances of the four numerical schemes. About 100 km downstream is the inlet of the Harrison Lake and there is no gauge station available at this location. The four numerical schemes are used to route the inflow hydrograph downstream for a distance of 100 km. Also for simplicity, the lateral inflows from the tributaries and the local drainage area are not taken into account and because there is no observed hydrograph exists at this location, the simulated hydrographs are also compared among themselves only.

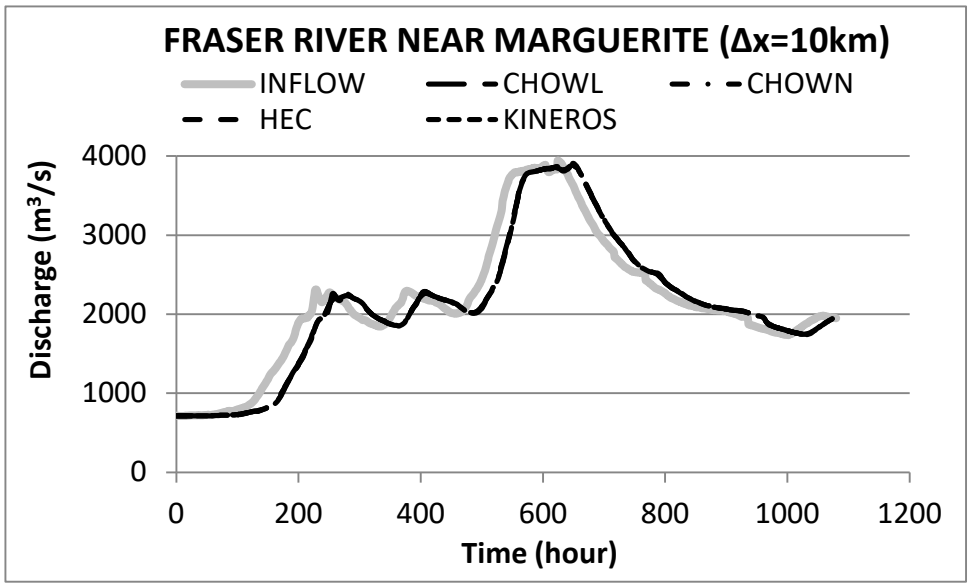

(a)

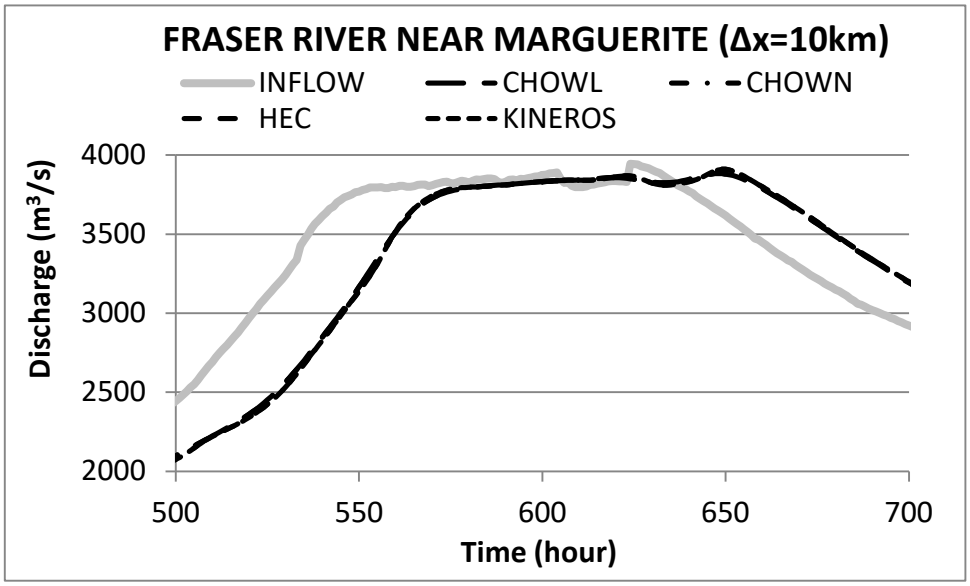

(b)

Figure 3. Comparison of output hydrographs for Scenario 1: [Δx = 10 km/ Δt = 1 h] and Scenario 2: [Δx = 20 km/ Δt = 1 h] for snowmelt flood inflow recorded at station Fraser River near Marguerite (08MC018). CHOWL represents Chow Linear and CHOWN represents Chow Nonlinear. (a) Complete hydrograph for Scenario 1, (b) peaking part for Scenario 1, (c) complete hydrograph for Scenario 2, and (d) peaking part for Scenario 2. (Continued next page.)

(c)

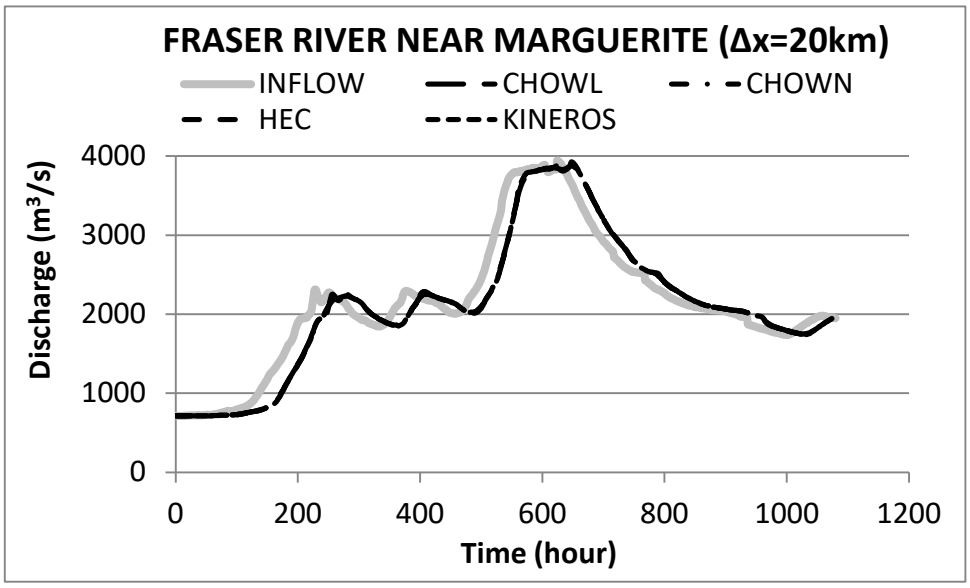

(d)

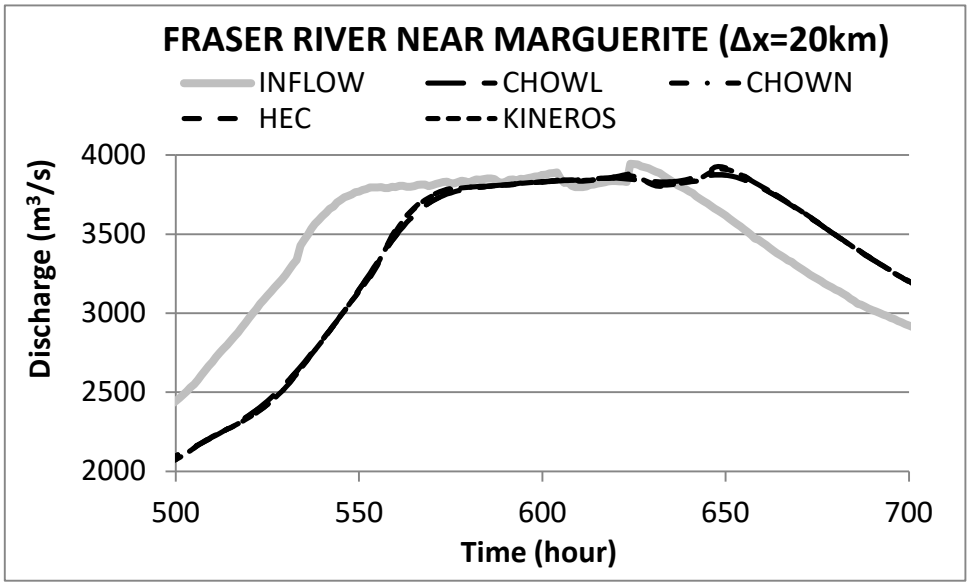

Figure 3. Comparison of output hydrographs for Scenario 1: [Δx = 10 km/ Δt = 1 h] and Scenario 2: [Δx = 20 km/ Δt = 1 h] for snowmelt flood inflow recorded at station Fraser River near Marguerite (08MC018). CHOWL represents Chow Linear and CHOWN represents Chow Nonlinear. (a) Complete hydrograph for Scenario 1, (b) peaking part for Scenario 1, (c) complete hydrograph for Scenario 2, and (d) peaking part for Scenario 2.

The river is assumed rectangular with the following parameters: width (b) = 50 m, slope (S0) = 0.001, and Manning's roughness coefficient (n) = 0.05. Considering the river length (100 km) and the minimum and maximum kinematic wave celerities (1.215 m/s and 3.678 m/s respectively) of the inflow hydrograph, the same two scenarios as the above are utilized to examine the performances of the four

schemes. Fig. 4 shows comparison of the output hydrographs from the four schemes, and (a) and (b) for Scenario 1 and (c) and (d) for Scenario 2. One can see from Fig. 4 that the deviations of the four output hydrographs from these four schemes for both scenarios are also small, though larger than those shown in Fig. 3, and the Chow Linear and Nonlinear schemes show larger numerical dispersion than the other two schemes, the HEC and KINEROS.

(a)

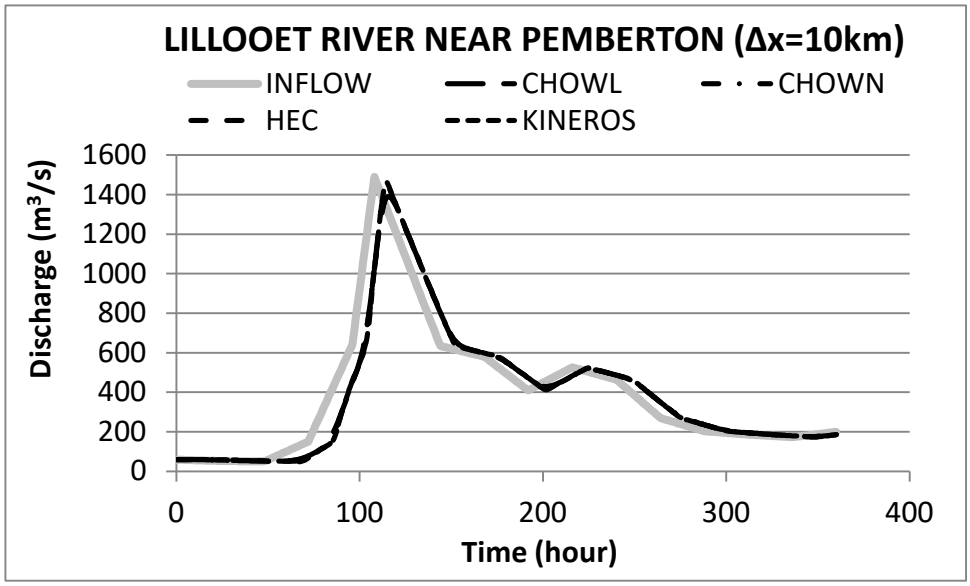

(b)

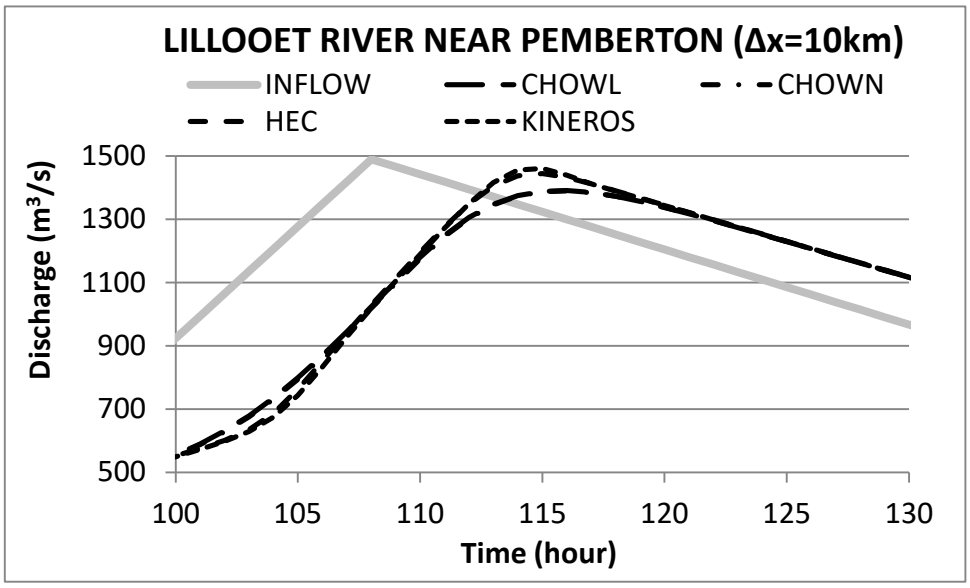

Figure 4. Comparison of output hydrographs for Scenario 1: [Δx = 10 km/ Δt = 1 h] and Scenario 2: [Δx = 20 km/ Δt = 1 h] for coastal storm flood inflow recorded at station Lillooet River near Pemberton (08MG005). CHOWL represents Chow Linear and CHOWN represents Chow Nonlinear. (a) Complete hydrograph for Scenario 1, (b) peaking part for Scenario 1, (c) complete hydrograph for Scenario 2, and (d) peaking part for Scenario 2. (Continued next page.)

(c)

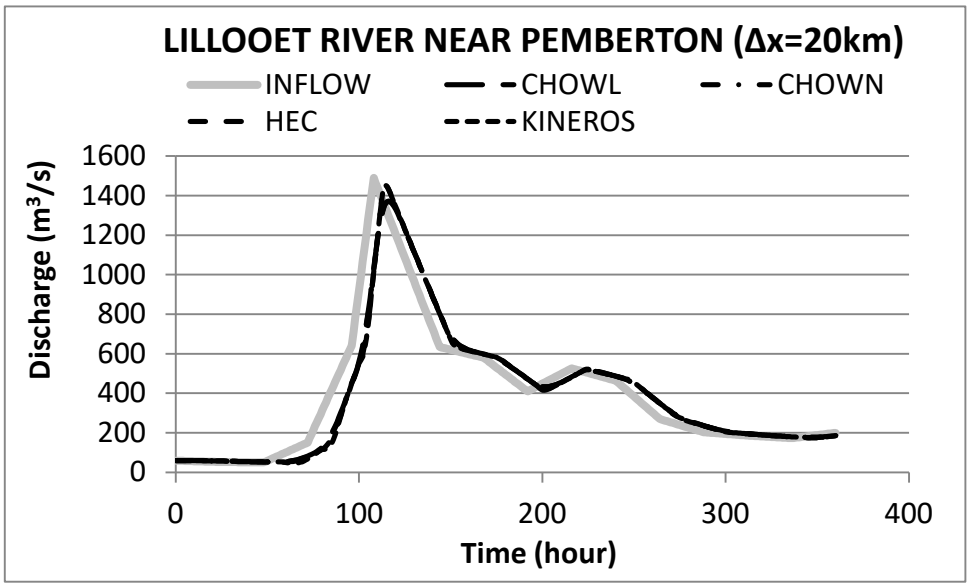

(d)

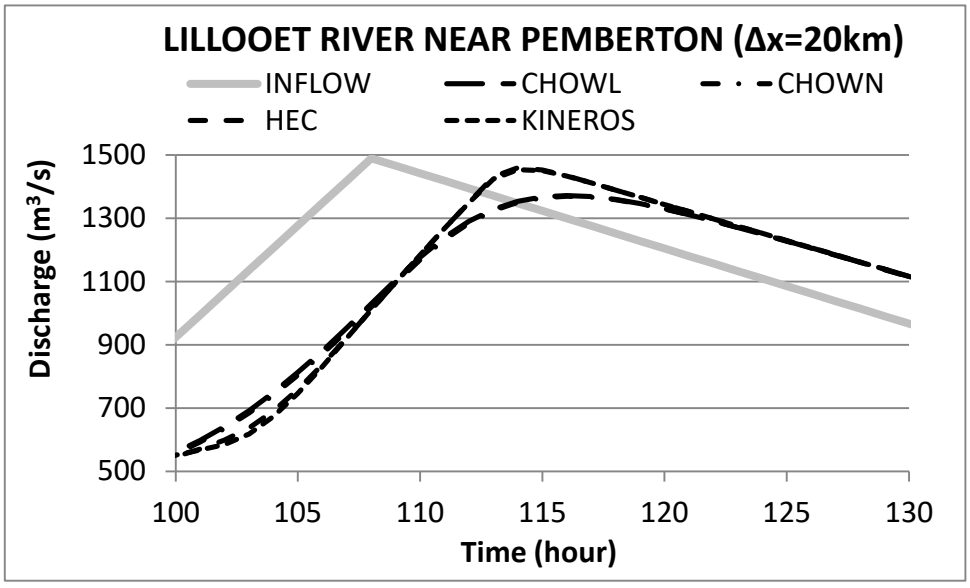

Figure 4. Comparison of output hydrographs for Scenario 1: [Δx = 10 km/ Δt = 1 h] and Scenario 2: [Δx = 20 km/ Δt = 1 h] for coastal storm flood inflow recorded at station Lillooet River near Pemberton (08MG005). CHOWL represents Chow Linear and CHOWN represents Chow Nonlinear. (a) Complete hydrograph for Scenario 1, (b) peaking part for Scenario 1, (c) complete hydrograph for Scenario 2, and (d) peaking part for Scenario 2.

The maximum deviations of the peak are 5.1% for Scenario 1 (between Chow Nonlinear and KINEROS) and 6.5% for Scenario 2 (between Chow Nonlinear and HEC), respectively. This means that all the four schemes perform closely enough for simulation of the fast rising (and fast dropping) coastal flood hydrographs though the Chow schemes demonstrate larger numerical dispersion than the other

two schemes.

The above comparisons of output hydrographs from the four numerical schemes demonstrate that the four numerical schemes perform similarly when they are utilized to route the natural flows of slow rising snowmelt floods and rapid rising coastal storm floods in the large-scale watersheds in BC though the Chow Linear and Nonlinear schemes tend to have larger numerical dispersion than the other two schemes, the HEC and KINEROS. The above results demonstrate that, with certain calibration efforts, these four numerical schemes are sufficient for the kinematic wave open channel routing for the natural floods from the snowmelt and coastal storms in BC's large-scale watersheds.

3.3. Routing regulated inflow and comparing model outputs with observation

In this subsection, the Chow Nonlinear scheme is dropped because its performance is very similar to that of the Chow Linear scheme. As such, the rest three numerical schemes, the Chow Linear, HEC and KINEROS, are further examined with the observed but regulated inflow and the output hydrographs from the three numerical schemes are compared with the observed flow at a downstream location.

The regulated WSC station Peace River at Hudson Hope (07EF001) recorded a very interesting hydrograph (Fig. 1 (c) is part of it) from February 12, 2016 to June 9, 2016, during which this manuscript is being prepared, and provides a rare opportunity to further examine the numerical schemes. The hydrograph shown in Fig. 1 (c) is selected as the inflow for the examination. This station is located about 8.5 km downstream of the Peace Canyon Dam which controls the downstream flow of the Peace River through human operations of its gates and spillways. The flow recorded at this station is observed but unnatural. About 150 km downstream is another WSC station, Peace River above Alces River (07FD010). The flow recorded at this downstream station for the same five day period (February 12, 2016 to February 16, 2016) is used to calibrate and verify the simulated hydrographs from the three numerical schemes. Between these two stations there are five major tributaries, which are, from upstream to downstream, the Halfway River, the Moberly River, the Pine River, the Beatton River and the Kiskatinaw River. During this period (February 12, 2016 to February 16, 2016) these tributaries flow at their base flows and the total is 33 m^3/s, which is only 2.2 % of the average flow recorded at the downstream station (07FD010) for this period. The local drainage area between these two stations is 6,240 km^2, which is only 5.2 % of the total drainage area (121,000 km^2) of the downstream station (07FD010), and the lateral inflow from this local drainage area is negligible because the snowmelt season has not started yet at this time. The three numerical schemes are employed to route the inflow recorded at the upstream station (07EF001) (as shown in Fig. 1 (c)). The river is assumed rectangular with the following parameters: width (b) = 100 m and slope (S_0) = 0.000743. And the Manning's roughness coefficient (n) is subject to calibration for each of the numerical schemes for Scenario SCN1, which will be defined below, so that the simulated hydrograph matches the observed one best for the scenario and for the scheme. The calibration results of the Manning's roughness coefficient (n) are 0.078 for Chow Linear, 0.075 for

HEC and 0.068 for KINEROS, respectively. The simulated hydrograph includes the outflow from each of the three numerical schemes plus the total base flow from all the major tributaries (33 m^3/s). The observed hydrograph is the flow recorded at the downstream station (07FD010). The time step is 1 hour and the scenarios are defined in Table 1. In order to examine the performances of the three numerical schemes to the greatest extent, these scenarios are so designed that the quotient of Δx/Δt covers a wide spectrum which ranges from a flow much smaller than the minimum kinematic wave celerity of the inflow (1.731 m/s) to that much larger than the maximum kinematic wave celerity of the inflow (2.77 m/s). Figs. 5 to 7 are the comparisons of the simulated hydrographs from the three numerical schemes and the observed flow recorded at the downstream station (07FD010).

Table 1. Scenarios SCN1 to SCN7 (Δt = 1 hour = 3600 s).

River Length (km)	Δx (km)	Δt (s)	Δx/Δt (m/s)	River Seg-ments	Scenario
150	1	3600	0.278	150	SCN1
	2.5		0.694	60	SCN2
	5		1.389	30	SCN3
	7.5		2.083	20	SCN4
	10		2.778	15	SCN5
	25		6.944	6	SCN6
	50		13.889	3	SCN7

Fig. 5 shows the comparison of the simulated hydrographs from the Chow Linear scheme for the seven scenarios and the observed hydrograph. Comparing Fig. 5 and Figs. 6 and 7, one can see that Chow Linear scheme has the greatest numerical dispersion for all scenarios among the three schemes, especially curtailing the reversed peaks (dips) considerably. Among the 7 scenarios, Scenario SCN1 (Δx = 1 km) has the best agreement between the simulated and observed hydrographs. Nevertheless, the model still cuts (overestimates) the reversed peaks (dips) by about 20 % for this scenario. This demonstrates the disability of the Chow Linear scheme (and Chow Nonlinear scheme as well) in routing this type of inflows by using a temporal increment as large as 1 hour or larger. Fig. 5 shows consistently that the numerical dispersion is positively correlated to the size of the spatial increment, or that the coarser the spatial increment, the larger the numerical dispersion, for both the peaks and reversed peaks (dips).

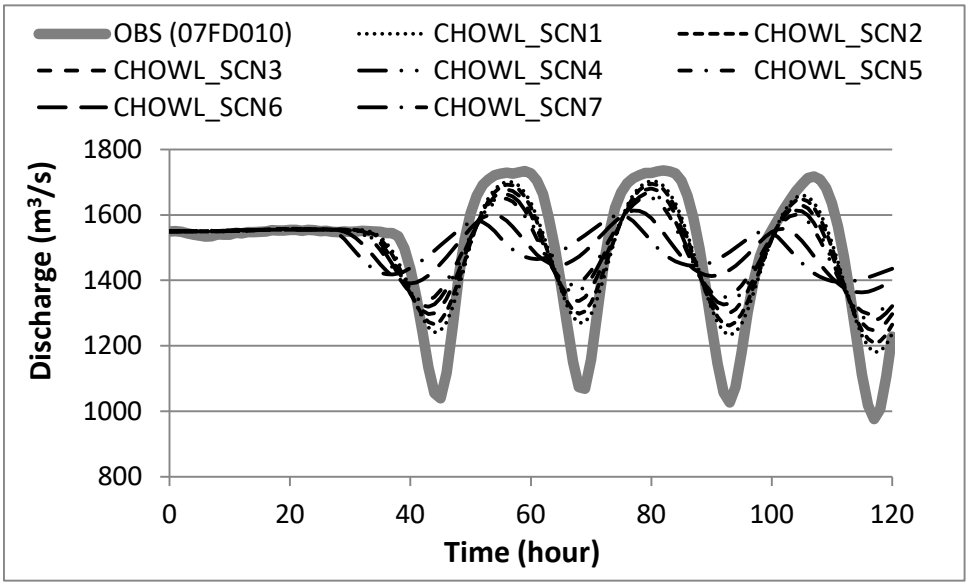

Figure 5. Comparison of simulated hydrographs from Chow Linear scheme (CHOWL) with observed hydrograph for Scenarios SCN1 to SCN7.

Fig. 6 (a) to (c) shows the comparison of the simulated hydrographs from the HEC scheme for the seven scenarios with the observed hydrograph. Fig. 6 shows a very interesting phenomenon that the simulated hydrographs from the HEC scheme fall into three completely different categories, (i) small numerical dispersion is present for both the peaks and the reversed peaks (dips) and the numerical dispersion is negatively correlated to the size of the spatial increment (the smaller the size, the larger the numerical dispersion) for Scenarios SCN1 to SCN3 (Fig. 6 (a)), (ii) odd solutions or large errors are present for Scenarios SCN4 and SCN5 (Fig. 6 (b)), and (iii) large numerical dispersion is present for both the peaks and reversed peaks (dips) and the numerical dispersion is positively correlated to the size of the spatial increment for Scenarios SCN6 and SCN7 (Fig. 6 (c)). Taking a close look at the scenarios, the causes for this phenomenon become clear. For Scenarios SCN1 to SCN3, $\Delta x/\Delta t <= 1.389$ m/s, which is smaller than the minimum kinematic wave celerity of the inflow (1.731 m/s) and therefore only the equations of the "conservation form" are used in the simulation based on HEC's equation selecting criterion. On the contrary for Scenarios SCN6 and SCN7, $\Delta x/\Delta t >= 6.944$ m/s, which is larger than the maximum kinematic wave celerity of the inflow (2.77 m/s) and as such only the equations of the "standard form" are used in the simulation based on HEC's equation selecting criterion. For Scenarios SCN4 and SCN5, $\Delta x/\Delta t$ (= 2.083 m/s and 2.778 m/s respectively) is between the minimum and maximum kinematic wave celerities and switching of equations between the conservation and standard forms becomes necessary in the simulation. And therefore, it can be concluded that the odd solutions or large errors are incurred by switching of equations between the two forms. The discrepancy of the "standard form" and the "conservation form" is so large under certain conditions that it is amplified gradually to

produce a big "jump" in the solution.

(a)

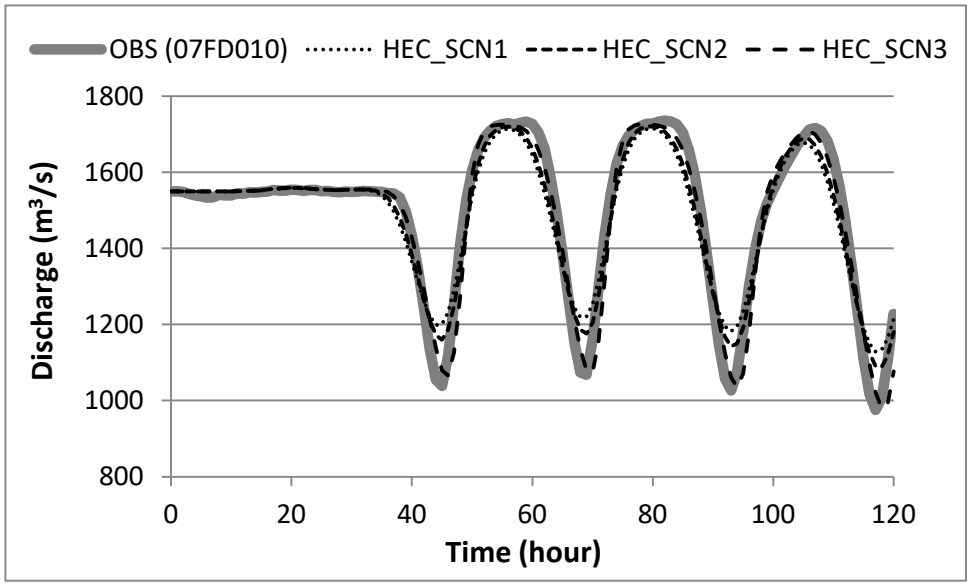

(b)

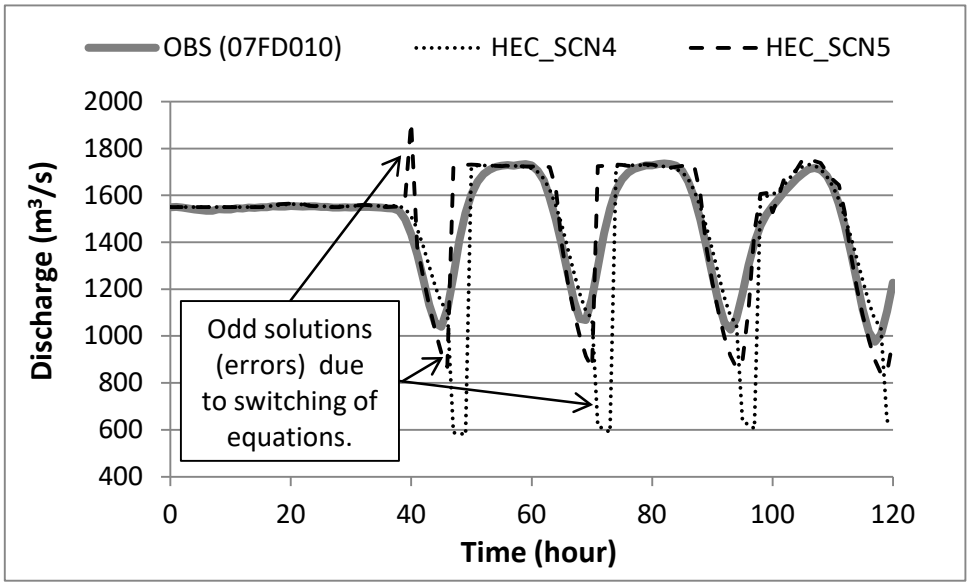

Figure 6. Comparison of simulated hydrographs from HEC scheme with observed hydrograph for Scenarios SCN1 to SCN7: (a) SCN1 to SCN3, (b) SCN4 and SCN5, and (c) SCN6 and SCN7. (Continued next page.)

(c)

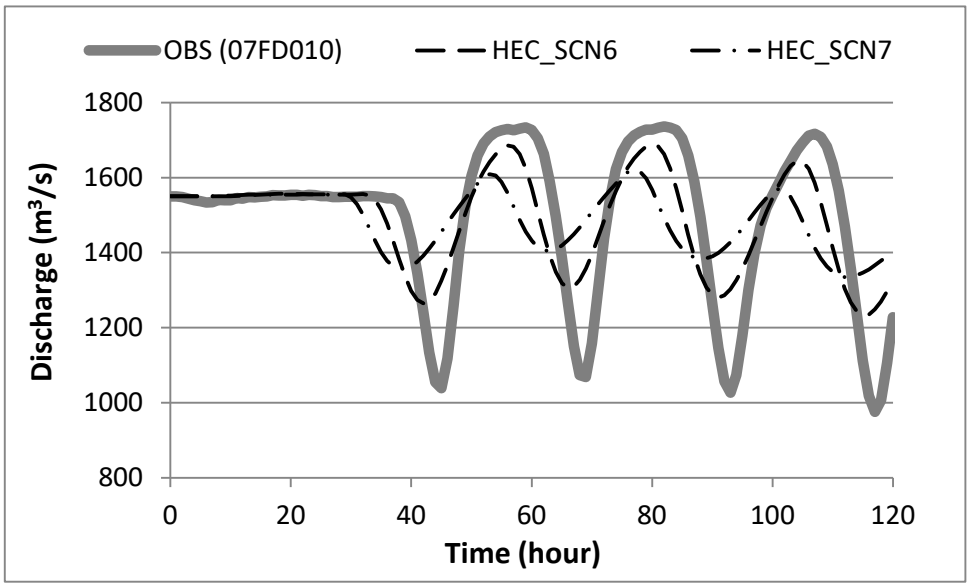

Figure 6. Comparison of simulated hydrographs from HEC scheme with observed hydrograph for Scenarios SCN1 to SCN7: (a) SCN1 to SCN3, (b) SCN4 and SCN5, and (c) SCN6 and SCN7.

Fig. 7 shows the comparison of the simulated hydrographs from the KINEROS scheme (θ=0.7) for the seven scenarios with the observed hydrograph. It is also interesting to see from Fig. 7 (a) that the simulated hydrographs from the KINEROS scheme for all the five scenarios have almost no numerical dispersion for the peaks and demonstrate, to the contrary of those from the Chow Linear scheme, "reversed numerical dispersion" for the reversed peaks (dips). Here, "reversed numerical dispersion" means that, rather than curtailing the reversed peaks (dips), the model extends the reversed peaks (dips) even further. Fig. 7 (a) shows that the extension of the reverse peaks (dips) is positively correlated to the size of the spatial increment. Fig. 7 (b) shows that oscillation is present for the two scenarios which have a larger size of the spatial increment even though the weighting factor (θ) is set to 0.7, which is the average value of the recommended range (0.6 to 0.8) by the KINEROS modeller. Fig. 7 (b) also shows large reversed numerical dispersion (extension) to the reverse peaks (dips) for the two scenarios.

Summarily, the examination in this subsection demonstrates that, for simulation of the observed regulated inflow shown in Fig. 1 (c) for a temporal increment of 1 hour or longer, the Chow Linear scheme (and the Chow Nonlinear scheme as well) is not appropriate due to large numerical dispersion, the HEC scheme is accurate only if the size of the spatial increment is so selected that the quotient of $\Delta x/\Delta t$ is close to and smaller than the minimum kinematic wave celerity of the inflow, and the KINEROS scheme is appropriate when the size of the spatial increment is small enough and the smaller, the better.

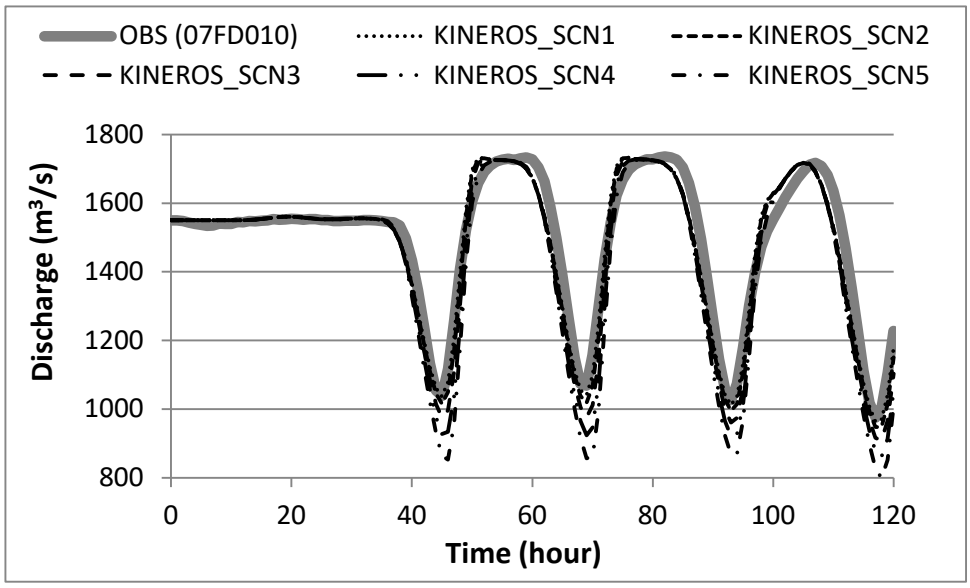

(a)

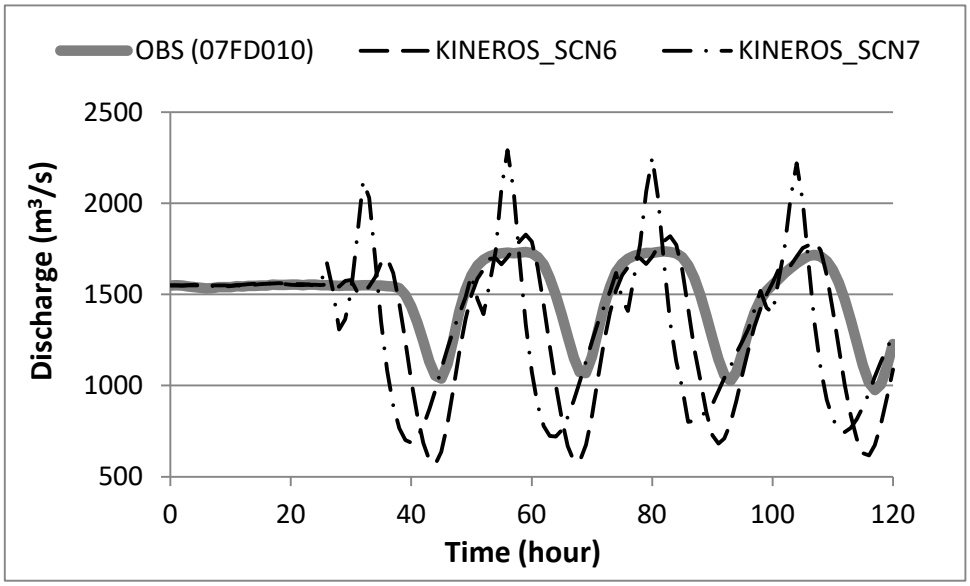

(b)

Figure 7. Comparison of simulated hydrographs from KINEROS scheme (θ=0.7) with observed hydrograph for Scenarios SCN1 to SCN7: (a) SCN1 to SCN5, and (b) SCN6 and SCN7.

4. Developing a new scheme for kinematic wave for BC large-scale watersheds

It is clear from the examinations in Subsection 3.3 that, in order to route the regulated hydrograph recorded at the WSC station Peace River at Hudson Hope (07EF001) (Fig.1 (c)) downstream with the kinematic wave, a new numerical scheme different from the four commonly used schemes becomes necessary. The new scheme should be stable and less-grid size dependent while maintaining reasonable accuracy. Stable means oscillation free. And less-grid size dependent means that the

numerical dispersion is less variable with the sizes of the temporal and spatial increments than that of the Chow schemes are. And reasonable accuracy means the new scheme dose not generate odd solutions or large errors under normal conditions. In this section, a new numerical scheme for the kinematic wave open channel routing is derived step by step.

4.1 Deriving the basic form

The kinematic wave simplification of the Saint Venant equations is given below when there is no lateral inflow:

$$\begin{cases} \frac{\partial Q}{\partial x} + \frac{\partial A}{\partial t} = 0 \\ S_0 = \frac{n^2 Q^2}{A^2 R^{4/3}} \end{cases} \tag{1}$$

in which Q is the discharge, x and t are the spatial and temporal coordinates respectively, A is the cross section area, S_0 is the channel slope, n is the Manning's roughness coefficient, and R is the hydraulic radius and is calculated with $R = A/P$, where P is the wet perimeter.

The Preissmann scheme (Preissmann, 1961) is commonly used to discretize the dynamic wave equations. However, in this study a finite difference scheme similar to the Preissmann scheme is adopted to discretize the continuity equation of the kinematic wave by setting the Preissmann spatial and temporal weighting coefficients to 0.5. The discretized continuity equation in Eq. 1 is written as:

$$\frac{1}{2\Delta x}\left[\left(Q_{i,j} - Q_{i-1,j}\right) + \left(Q_{i,j-1} - Q_{i-1,j-1}\right)\right] +$$

$$\frac{1}{2\Delta t}\left[\left(A_{i,j} - A_{i,j-1}\right) - \left(A_{i-1,j} - A_{i-1,j-1}\right)\right] = 0 \tag{2}$$

in which i and j denote the spatial and temporal steps on the x and y coordinates respectively and (i, j) is the unknown node, and Δx and Δt are the spatial and temporal increments respectively.

Discretizing and rearranging the momentum equation in Eq. (1) produces:

$$Q_{i,j} = \frac{1}{n}\sqrt{S_0} R_{i,j}^{2/3} A_{i,j} \tag{3}$$

Define:

$$V_{i,j} = \frac{1}{n}\sqrt{S_0} R_{i,j}^{2/3} \tag{4}$$

and substitute Eq. (4) into Eq. (3), which becomes:

$$Q_{i.j} = V_{i,j} A_{i,j} \tag{5}$$

Substituting Eq. (5) into Eq. (2) with some rearrangements gives:

$$A_{i,j} = \frac{\Delta t\left(Q_{i-1,j} + Q_{i-1,j-1} - Q_{i,j-1}\right) + \Delta x\left(A_{i,j-1} + A_{i-1,j-1} - A_{i-1,j}\right)}{\Delta t V_{i,j} + \Delta x} \tag{6}$$

If $V_{i,j}$ is known so that Eq. (6) can be solved, substitute the result of $A_{i,j}$ into Eq. (5) and $Q_{i,j}$ can be

found. However, Eq. (6) is unsolvable because $V_{i,j}$ is also an unknown.

In order to solve Eq. (6), an efficient iteration scheme similar to the Semi-Implicit Method for Pressure-Linked Equations (SIMPLE) (Patankar and Spalding, 1972) is introduced. The SIMPLE is an optimized numerical scheme which solves pressure related equations iteratively with high accuracy because that it is able to avoid water balance errors and the divergence problem (Luo, 2007), and therefore the SIMPLE scheme was adopted to solve the diffusive-wave governing equations of the fully distributed, physics-based watershed model – LUOM (Luo, 2007). Pressure is a concept in fluid dynamics and the relevant concept in hydrology is water head or water depth (Luo, 2007). In this study, the cross section of the open channel is assumed rectangular and therefore (h is the water depth and b is the channel width):

$$A = bh \tag{7}$$

$$\begin{cases} P = b + 2h \\ R = A/P \end{cases} \tag{8}$$

Or in a simplified form:

$$R_{i,j} = f\left(h_{i,j}\right) \tag{9}$$

At the beginning of the iteration, the initial value of the water depth is set to the water depth of the previous time step:

$$\left(h_{i,j}\right)^{(0)} = h_{i,j-1} \tag{10}$$

Substituting Eq. (10) into Eq. (9) yields:

$$\left(R_{i,j}\right)^{(0)} = f\left(\left(h_{i,j}\right)^{(0)}\right) \tag{11}$$

Substituting Eq. (11) into Eq. (4) gives:

$$\left(V_{i,j}\right)^{(0)} = \frac{1}{n}\sqrt{S_0}\left(\left(R_{i,j}\right)^{(0)}\right)^{2/3} \tag{12}$$

With this initial value of $V_{i,j}$, Eq. (6) is rewritten as:

$$\left(A_{i,j}\right)^{(1)} = \frac{\Delta t\left(Q_{i-1,j}+Q_{i-1,j-1}-Q_{i,j-1}\right)+\Delta x\left(A_{i,j-1}+A_{i-1,j-1}-A_{i-1,j}\right)}{\Delta t\left(V_{i,j}\right)^{(0)}+\Delta x} \tag{13}$$

In Eqs. (10) to (13), superscript (0) means that the value of the variable in the parentheses before it is the initial value, and superscript (1) means that the value of the variable in the parentheses before it is the value found in the iteration step 1, and so on. If k-1 and k are used to denote the previous and the current iteration steps, the general form of the iteration equation for Eq. 6 is written as:

$$\left(A_{i,j}\right)^{(k)} = \frac{\Delta t\left(Q_{i-1,j}+Q_{i-1,j-1}-Q_{i,j-1}\right)+\Delta x\left(A_{i,j-1}+A_{i-1,j-1}-A_{i-1,j}\right)}{\Delta t\left(V_{i,j}\right)^{(k-1)}+\Delta x} \tag{14}$$

After Eq. (14) is solved at iteration step k, a new initial value of water depth $\left(h_{i,j}\right)^{(k)}$ for the new

iteration step (k+1) will be found by following the steps below. First, substitute the result from Eq. (14) into Eq. (7) and rearrange it:

$$\left(h_{i,j}\right)^{(k0)} = \left(A_{i,j}\right)^{(k)}/b \tag{15}$$

Then the correction (h') to the initial value of water depth is found as below:

$$h'_{i,j} = \left(h_{i,j}\right)^{(k0)} - \left(h_{i,j}\right)^{(k-1)} \tag{16}$$

The new initial value of water depth for the next iteration step (k+1) is calculated with the following equation:

$$\left(h_{i,j}\right)^{(k)} = \left(h_{i,j}\right)^{(k-1)} + \alpha h'_{i,j} \tag{17}$$

where α is the so-called under-relaxation factor which varies from 0 to 1. Use $\left(h_{i,j}\right)^{(k)}$ to calculate $\left(V_{i,j}\right)^{(k)}$ and then substitute $\left(V_{i,j}\right)^{(k)}$ into Eq. (14), and so on until that h' approaches 0 or a small value of the desired accuracy.

Now the kinematic wave equation is solved by Eq. (14) iteratively. However, the Preissmann scheme (Preissmann, 1961) is a second order scheme if both the spatial and temporal weighting coefficients are equal to 0.5 (Meselhe and Holly, 1997). This is the case in this study. Meselhe and Holly (1997) found that this scheme is unconditional stable for the dynamic wave. However, it is unstable for the kinematic wave. An examination of this scheme is carried out by running Scenario SCN1 defined in Subsection 3.3. Fig. 8 shows that the simulated hydrograph includes oscillations in the peaks.

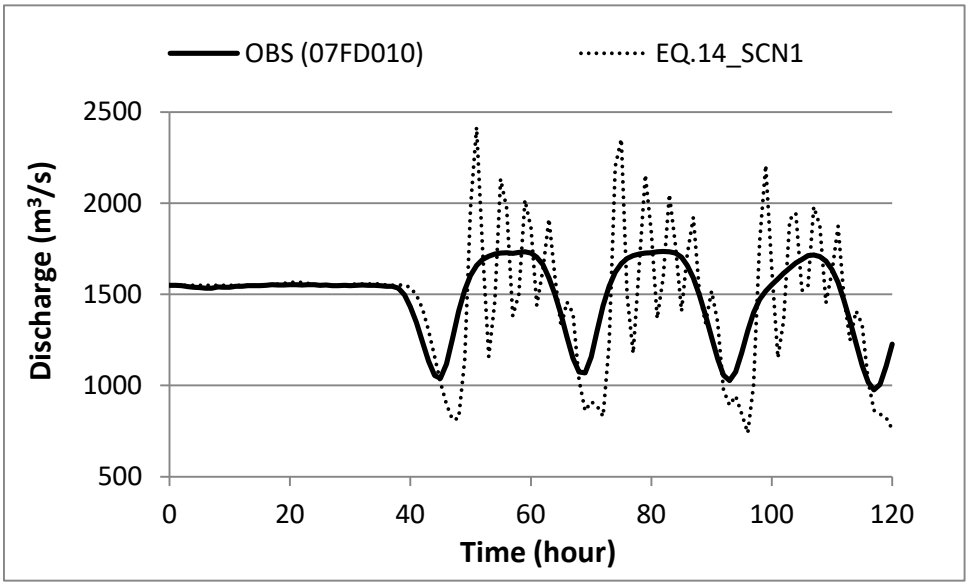

Figure 8. Oscillation present in simulated hydrograph (EQ.14_SCN1) from Eq. (14).

In order to obtain a total variation diminishing (TVD) or oscillation free scheme (Harten, 1983; Sweby, 1984), a flux limiter must be introduced to Eqs. (6) and (14). Setting both the Preissmann spatial and temporal weighting coefficients to 1, the Preissmann scheme reduces to an implicit first order scheme:

$$\frac{1}{\Delta x}\left(Q_{i,j} - Q_{i-1,j}\right) + \frac{1}{\Delta t}\left(A_{i,j} - A_{i,j-1}\right) = 0 \tag{18}$$

Substituting Eq. (5) into Eq. (18) with some rearrangements produces:

$$A_{i,j} = \frac{\Delta t Q_{i-1,j} + \Delta x A_{i,j-1}}{\Delta t V_{i,j} + \Delta x} \tag{19}$$

This is the first order form of Eq. (6). Comparing Eq. (6) with this first order form and after some rearrangements, Eq. (6) becomes:

$$A_{i,j} = \frac{\Delta t Q_{i-1,j} + \Delta x A_{i,j-1}}{\Delta t V_{i,j} + \Delta x} + \frac{\Delta t\left(Q_{i-1,j-1} - Q_{i,j-1}\right) + \Delta x\left(A_{i-1,j-1} - A_{i-1,j}\right)}{\Delta t V_{i,j} + \Delta x} \tag{20}$$

in which the first term on the right-hand side is the first order term and the second term is the anti-diffusive flux term. Applying a non-negative flux limiter $\varphi(r)$ (r is the ratio of the consecutive gradients or the smoothness parameter) to the anti-diffusive flux term, Eq. (20) becomes:

$$A_{i,j} = \frac{\Delta t Q_{i-1,j} + \Delta x A_{i,j-1}}{\Delta t V_{i,j} + \Delta x} + \varphi\left(r_{ij}\right)\frac{\Delta t\left(Q_{i-1,j-1} - Q_{i,j-1}\right) + \Delta x\left(A_{i-1,j-1} - A_{i-1,j}\right)}{\Delta t V_{i,j} + \Delta x} \tag{21}$$

Eq. (21) can be solved iteratively by following the same steps from Eq. (7) to Eq. (17) and replacing Eq. (14) with the following iteration equation for Eq. (21):

$$\left(A_{i,j}\right)^{(k)} = \frac{\Delta t Q_{i-1,j} + \Delta x A_{i,j-1}}{\Delta t\left(V_{i,j}\right)^{(k-1)} + \Delta x} + \varphi\left(r_{ij}\right)\frac{\Delta t\left(Q_{i-1,j-1} - Q_{i,j-1}\right) + \Delta x\left(A_{i-1,j-1} - A_{i-1,j}\right)}{\Delta t\left(V_{i,j}\right)^{(k-1)} + \Delta x} \tag{22}$$

Eqs. (21) and (22) are TVD or oscillation free if an appropriate flux limiter is found.

4.2 Selecting an appropriate flux limiter

In this study, uniform initial conditions are applied to the open channel and coarser spatial increments are preferable for time efficiency of modeling in the large-scale watersheds in BC. Because of the latter, the minimum number of channel segments can be as few as two in some of the watersheds. Therefore in this study, the ratio of consecutive gradients (r) is not defined along the spatial axis, but rather defined on the temporal axis and given by:

$$r_{i,j} = \frac{Q_{i-1,j-1} - Q_{i-1,j-2}}{Q_{i-1,j} - Q_{i-1,j-1}} \tag{23}$$

Sweby (1984) had provided an analysis and comparison of a number of flux limiters which include Van Leer (1974), Roe (1981), Chakravarthy and Osher (1983) and one presented by the author. Besides those included in Sweby (1984), some other flux limiters also had been existing or have become existing later. In this study in order to find the most appropriate flux limiter for Eq. (21) or (22), a total of nine

different flux limiters are selected to test the solution of Eq. (22):

(1) Minmod (Roe, 1981; 1986):

$$\varphi(r) = max[0, min(1, r)] \tag{24}$$

(2) Superbee (Roe, 1981; 1986):

$$\varphi(r) = max[0, min(2r, 1), min(r, 2)] \tag{25}$$

(3) Van Leer (1974):

$$\varphi(r) = \frac{r+|r|}{1+|r|} \tag{26}$$

(4) Osher (Chakravarthy and Osher, 1983):

$$\varphi(r) = max[0, min(r, \beta)],\ 1 \le \beta \le 2\ (\beta = 1.5 \text{ in this study}) \tag{27}$$

(5) Van Albada 1 (Van Albada et al., 1982):

$$\varphi(r) = \frac{r^2+r}{r^2+1} \tag{28}$$

(6) Sweby (1984):

$$\varphi(r) = max[0, min(\beta r, 1), min(r, \beta)],\ 1 \le \beta \le 2\ (\beta = 1.5 \text{ in this study}) \tag{29}$$

(7) Ospre (Waterson and Deconinck, 1995):

$$\varphi(r) = \frac{1.5(r^2+r)}{r^2+r+1} \tag{30}$$

(8) Monotonized Central (Van Leer, 1977):

$$\varphi(r) = max[0, min(2r, 0.5(1+r), 2)] \tag{31}$$

(9) UMIST (Lien and Leschziner, 1994):

$$\varphi(r) = max[0, min(2r, (0.25+0.75r), (0.75+0.25r), 2)] \tag{32}$$

Eqs. (24) to (32) are substituted into Eq. (22) one by one and the equation is used to simulate the seven scenarios given in Subsection 3.3. The Manning's roughness coefficient (n) is set to 0.062 so that Scenario SCN1 is best calibrated for all the flux limiters. Fig. 9 shows the output hydrographs from the solution of Eq. (22) by using the above different flux limiters. One can see visually from Fig. 9 that the simulated hydrograph by using the flux limiter Minmod (Roe, 1981; 1986) (Fig. 9 (a)) is the best in respect of diminishing the oscillation for all the seven scenarios.

In order to obtain a more objective judgement, a number of statistical indicators are employed to evaluate the simulated hydrographs shown in Fig. 9 by comparing them with the observed hydrograph. These statistical indicators include: (1) the coefficient of model efficiency (Ce), which describes how well the volume and timing of the simulated hydrograph compares to the observed hydrograph, and the closer to 1 the value is, the better the simulated hydrograph fits the observed hydrograph (Nash and Sutcliffe, 1970), (2) the coefficient of model determination (Cd), which measures how well the shape of the simulated hydrograph reflects the observed hydrograph and depends solely on the timing of changes in the hydrograph, and the closer to 1 the value is, the better the simulated hydrograph fits the

observed hydrograph (Nash and Sutcliffe, 1970), (3) the percentage volume difference (dV) of the simulated hydrograph relative to the observed hydrograph (Nash and Sutcliffe, 1970), (4) the relative mean absolute error (Era) of the simulated hydrograph to the observed hydrograph (Lettenmaier and Wood, 1992), and (5) the square of the Pearson product moment correlation coefficient between the simulated and observed hydrographs – r squared (r^2), and the closer to 1 the value is, the better the simulated hydrograph fits the observed hydrograph.

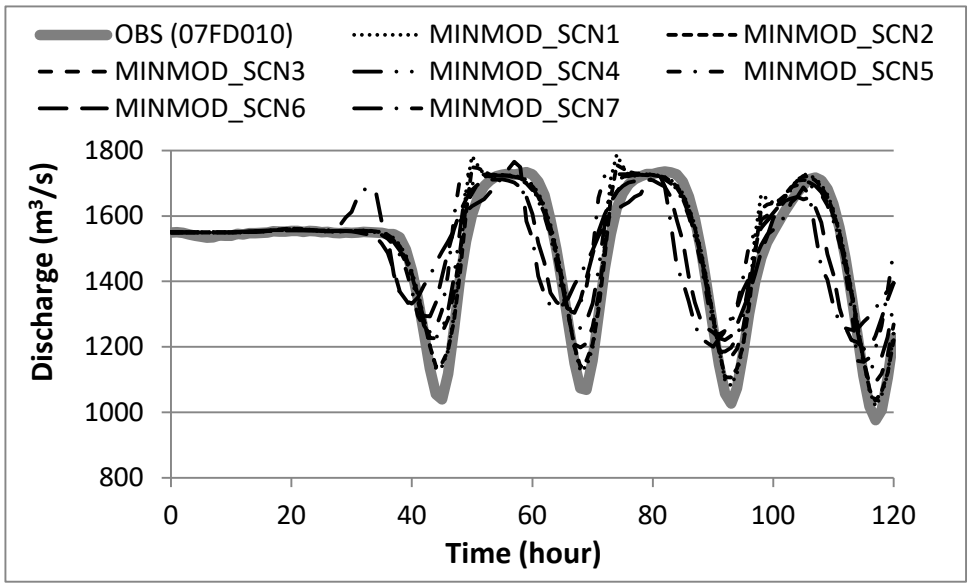

(a)

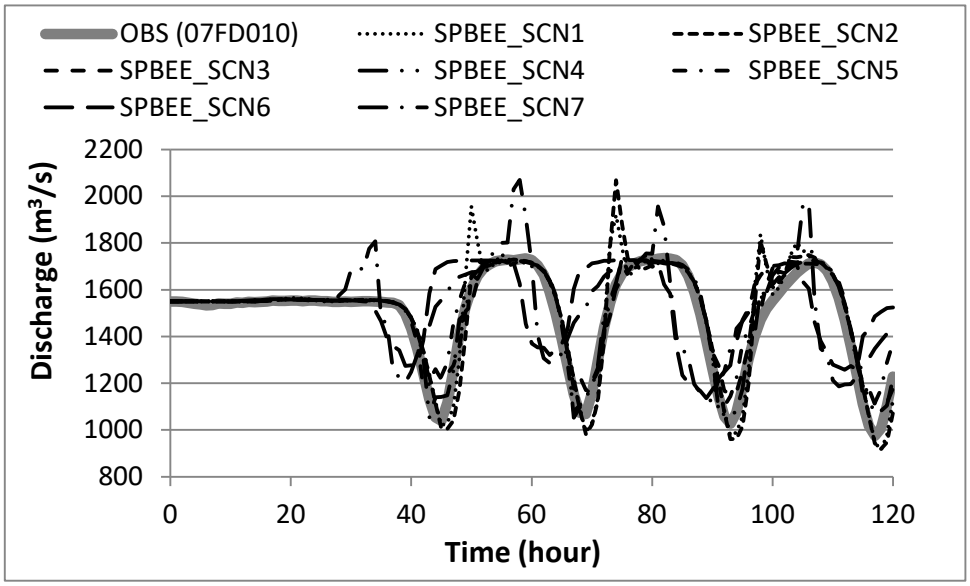

(b)

Figure 9. Simulated hydrographs from solution of Eq. (22) for SCN1 to SCN7 by using flux limiters: (a) Minmod, (b) Superbee, (c) Van Leer, (d) Osher, (e) Van Albada 1, (f) Sweby, (g) Ospre, (h) Monotonized Central, and (i) UMIST. (Continued next pages.)

(c)

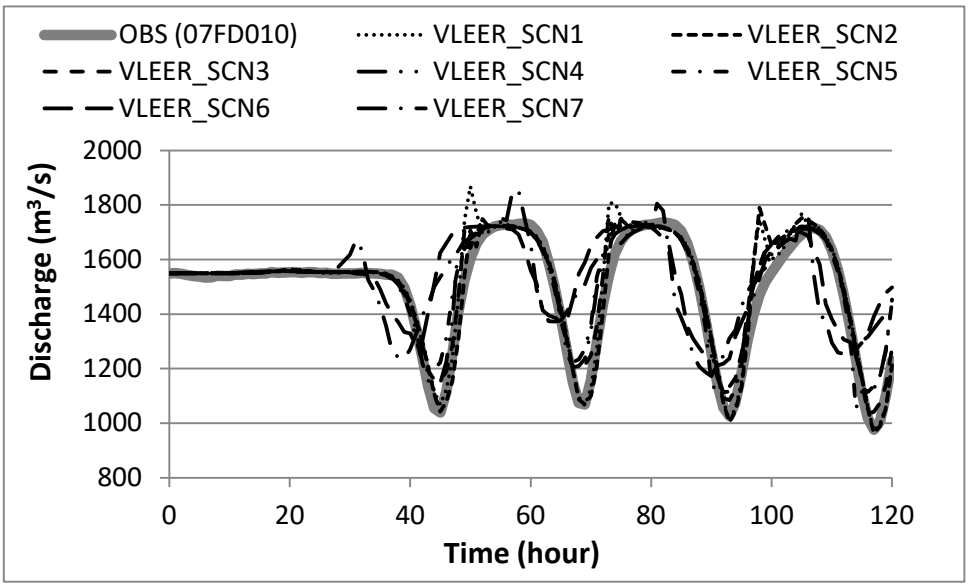

(d)

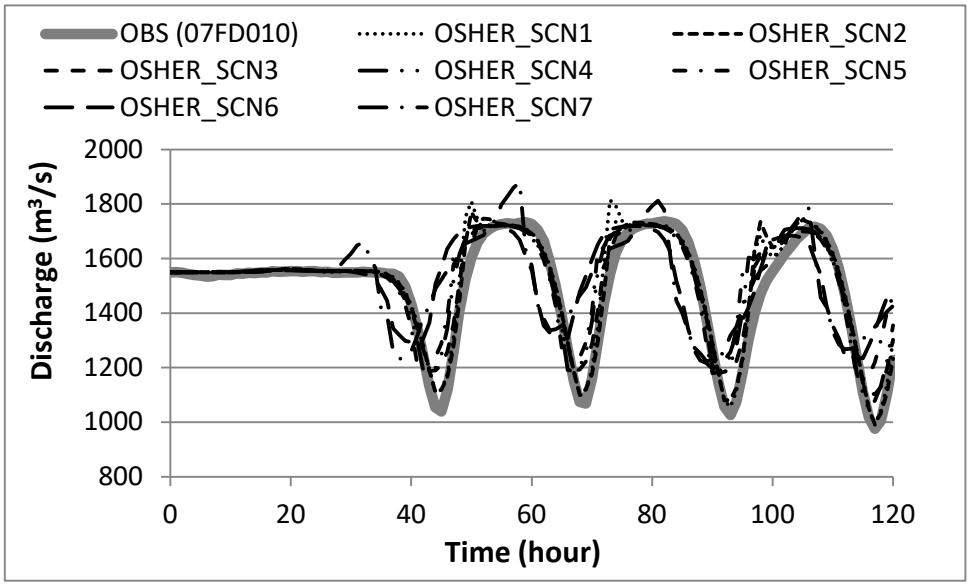

Figure 9. Simulated hydrographs from solution of Eq. (22) for SCN1 to SCN7 by using flux limiters: (a) Minmod, (b) Superbee, (c) Van Leer, (d) Osher, (e) Van Albada 1, (f) Sweby, (g) Ospre, (h) Monotonized Central, and (i) UMIST. (Continued next pages.)

(e)

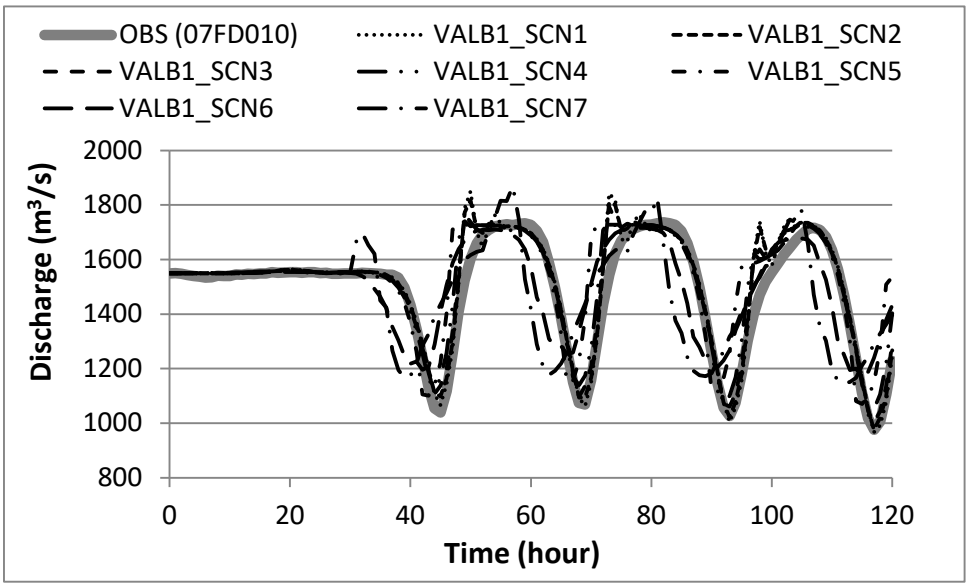

(f)

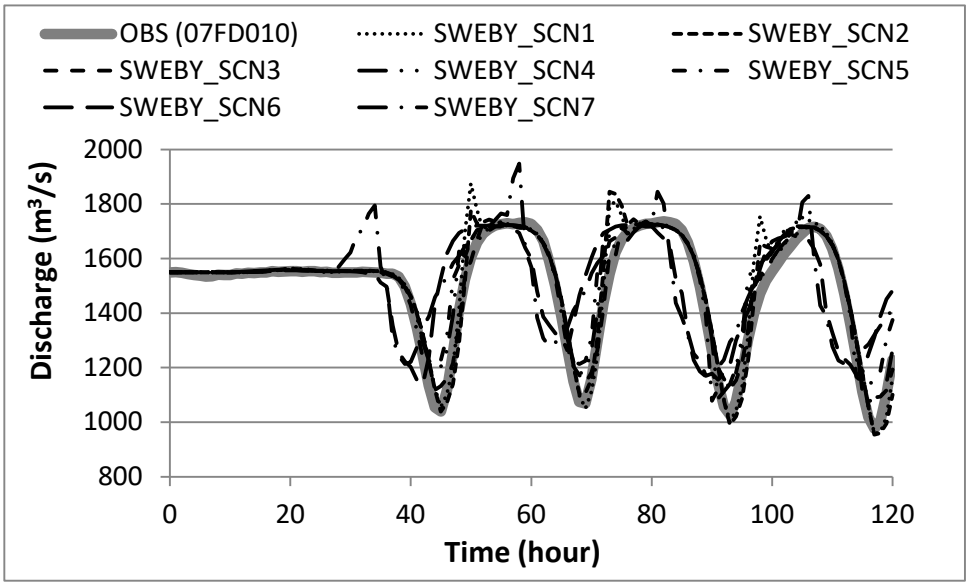

Figure 9. Simulated hydrographs from solution of Eq. (22) for SCN1 to SCN7 by using flux limiters: (a) Minmod, (b) Superbee, (c) Van Leer, (d) Osher, (e) Van Albada 1, (f) Sweby, (g) Ospre, (h) Monotonized Central, and (i) UMIST. (Continued next pages.)

(g)

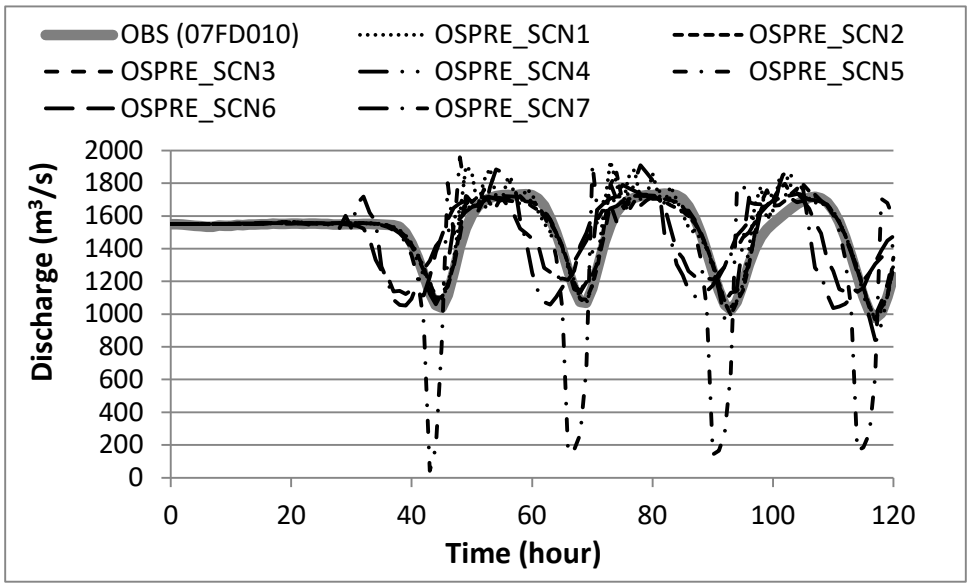

(h)

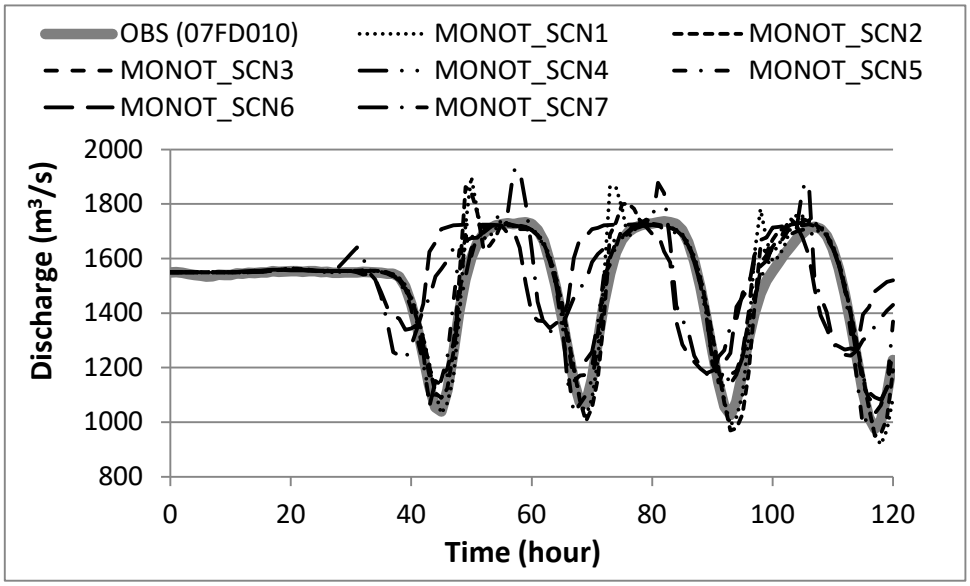

Figure 9. Simulated hydrographs from solution of Eq. (22) for SCN1 to SCN7 by using flux limiters: (a) Minmod, (b) Superbee, (c) Van Leer, (d) Osher, (e) Van Albada 1, (f) Sweby, (g) Ospre, (h) Monotonized Central, and (i) UMIST. (Continued next page.)

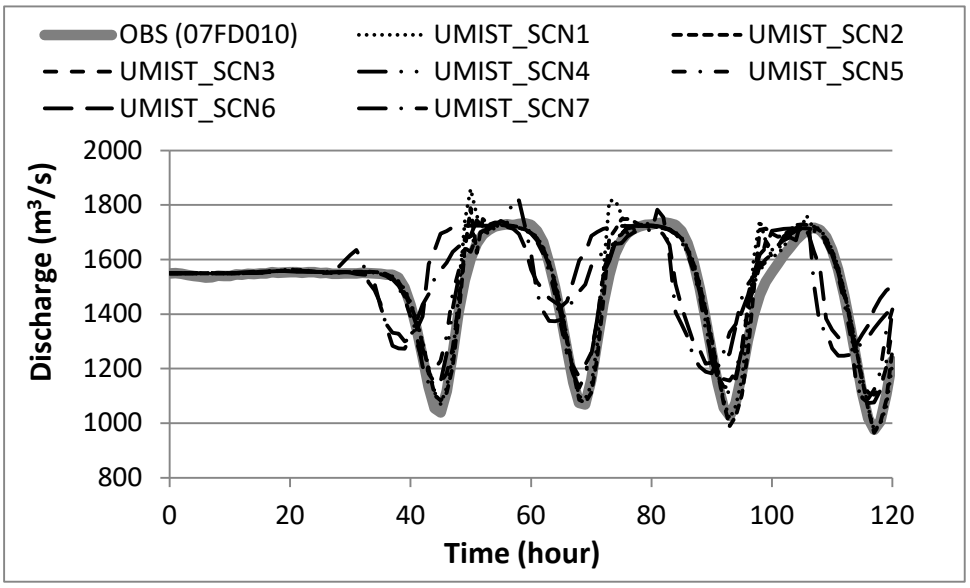

(i)

Figure 9. Simulated hydrographs from solution of Eq. (22) for SCN1 to SCN7 by using flux limiters: (a) Minmod, (b) Superbee, (c) Van Leer, (d) Osher, (e) Van Albada 1, (f) Sweby, (g) Ospre, (h) Monotonized Central, and (i) UMIST.

Table 2 lists the evaluation results of the simulated hydrographs for the nine flux limiters for Scenario SCN1. It can be seen from Table 2 that the simulated hydrograph by using the Minmod flux limiter has the largest (best) Ce, Cd and r squared, the third smallest (best) of dV and the second smallest (best) Era. These statistics concur with the visual evaluation of Fig. 9. As the result of the above visual and statistical evaluations, Eq. (24) - Minmod (Roe, 1981; 1986) is selected as the flux limiter for Eqs. (21) and (22).

Table 2. Statistics of simulated hydrographs for Scenario SCN1 from solution of Eq. (22) using nine flux limiters.

FLUX LIMITER (SCN1)	Ce	Cd	dV (%)	Era (%)	RSQ
1. Minmod	0.941	0.955	1.613	2.110	0.955
2. Supperbee	0.838	0.885	1.523	3.376	0.885
3. Van Leer	0.912	0.929	1.622	2.165	0.929
4. Osher	0.915	0.931	1.760	2.274	0.931
5. Van Albada 1	0.904	0.920	1.618	2.279	0.920
6. Sweby	0.906	0.927	1.652	2.431	0.927
7. Ospre	0.797	0.846	2.360	3.559	0.846
8. Monotonized Central	0.877	0.907	1.406	2.719	0.907
9. UMIST	0.913	0.929	1.634	2.109	0.929

Note: RSQ - r squared, SCN1 - Scenario SCN1.

4.3 Comparing with other schemes

Comparing Fig. 9 (a) with Figs. (5), (6) and (7), one can see visually that the scheme developed in the above subsections has smaller magnitude of numerical dispersion than the Chow Linear scheme, no odd solutions or large errors as the HEC scheme does incurred by switching of equations for scenarios of certain sizes of the spatial increment, and no oscillation as the KINEROS scheme does when the size of the spatial increment increases.

The scheme developed in this study is also compared statistically with the Chow Linear, HEC and KINEROS schemes by using the same statistical indicators as used in Table 2: the coefficient of model efficiency (Ce), the coefficient of model determination (Cd), the percentage volume difference (dV), the relative mean absolute error (Era) and r squared. Table 3 lists the statistics of the simulated hydrographs from the schemes of this study, Chow Linear, HEC and KINEROS compared with the observed hydrograph. One can see from Table 3 that Ce, Cd and r squared for the Chow Linear scheme decrease quickly to very small values for Scenarios SCN6 and SCN7 due to numerical dispersion, while Ce of the HEC scheme becomes negative for Scenario SCN4 due to the large errors incurred by switching of equations and Ce, Cd and r squared for the HEC scheme also become very small for Scenario SCN7 because of numerical dispersion, and Ce of the KINEROS scheme becomes negative for both Scenarios SCN6 and SCN7 because of the oscillation and reversed numerical dispersion and Cd and r squared for Scenario SCN7 also drop to very small values and Era for Scenario SCN7 is the largest (16.7%) among all the schemes for all scenarios. One also can see from Table 3 that, comparing with the other schemes, the scheme developed in this study has more evenly distributed and thus less grid-size (of the spatial increment) dependent statistics, which are better than those of the other schemes for some, though not all, scenarios. And therefore overall, the scheme developed in this study is better than the other schemes for open channel routing in BC's large-scale watershed modeling, in which it is difficult to change frequently the size of the spatial increment based on the inflow.

In order to further examine the applicability of the scheme developed in this study, similar seven scenarios with a shorter temporal increment (5 minutes) are composed for the same inflow and channel conditions described in Subsection 3.3. Similarly, the scenarios are so designed that the quotient of $\Delta x/\Delta t$ covers a wide spectrum of celerity which ranges from that much smaller than the minimum kinematic wave celerity of the inflow (1.731 m/s) to that much larger than the maximum kinematic wave celerity of the inflow (2.77 m/s). Table 4 listed the seven scenarios. Fig. 10 shows the simulated hydrographs output from the scheme developed in this study and the schemes of Chow Linear, HEC and KINEROS. Table 5 gives the statistics of the simulated hydrographs compared with the observed hydrograph.

Table 3. Statistics of simulated hydrographs from schemes of this study, Chow Linear, HEC and KINEROS for sever scenarios.

Scheme	Scenario	Ce	Cd	dV (%)	Era (%)	RSQ
LUO	SCN1	0.941	0.955	1.613	2.110	0.955
(This study)	SCN2	0.955	0.967	1.346	1.997	0.967
	SCN3	0.927	0.962	1.656	2.514	0.962
	SCN4	0.873	0.926	2.147	3.215	0.926
	SCN5	0.671	0.741	3.271	4.867	0.741
	SCN6	0.593	0.601	0.864	5.972	0.601
	SCN7	0.355	0.365	0.991	7.678	0.365
CHOW LINEAR	SCN1	0.850	0.919	-0.111	3.890	0.919
	SCN2	0.804	0.898	0.050	4.425	0.898
	SCN3	0.727	0.855	0.242	5.204	0.855
	SCN4	0.655	0.805	0.375	5.866	0.805
	SCN5	0.588	0.749	0.472	6.413	0.749
	SCN6	0.294	0.380	0.741	8.583	0.380
	SCN7	0.028	0.038	0.869	10.270	0.038
HEC	SCN1	0.906	0.939	-0.338	3.074	0.939
(Combined	SCN2	0.942	0.958	-0.370	2.443	0.958
standard and	SCN3	0.953	0.955	-0.444	1.995	0.955
conservation	**SCN4**	**-0.216**	**0.502**	**-2.519**	**6.586**	**0.502**
forms)	SCN5	0.694	0.840	0.999	4.208	0.840
	SCN6	0.664	0.716	-0.294	5.730	0.716
	SCN7	0.176	0.177	-0.229	9.414	0.177
KINEROS	SCN1	0.943	0.956	-0.924	2.408	0.956
(θ=0.7)	SCN2	0.932	0.958	-1.356	2.716	0.958
	SCN3	0.898	0.958	-2.141	3.273	0.958
	SCN4	0.837	0.955	-3.032	3.982	0.955
	SCN5	0.733	0.950	-4.068	4.823	0.950
	SCN6	**-0.320**	**0.846**	**-8.798**	**10.445**	**0.846**
	SCN7	**-2.180**	**0.228**	**-9.350**	**16.736**	**0.228**

Note: RSQ - r squared.

Table 4. Scenarios SCN11 to SCN17 (Δt = 5 minutes).

River Length (km)	Δx (km)	Δt (s)	Δx/Δt (m/s)	River Segments	Scenario
150	0.25	300	0.833	600	SCN11
	0.50		1.667	300	SCN12
	0.75		2.500	200	SCN13
	1		3.333	150	SCN14
	2.5		8.333	60	SCN15
	5		16.667	30	SCN16
	10		33.333	15	SCN17

Table 5. Statistics of simulated hydrographs from scheme developed in this study and schemes of Chow Linear, HEC and KINEROS for SCN11 to SCN17.

Scheme	Scenario	Ce	Cd	dV (%)	Era (%)	RSQ
LUO	SCN11	0.473	0.727	1.053	4.778	0.727
(This study)	SCN12	0.521	0.740	1.314	4.635	0.740
	SCN13	0.575	0.745	2.075	4.489	0.745
	SCN14	0.575	0.742	2.252	4.502	0.742
	SCN15	0.630	0.783	1.690	4.236	0.783
	SCN16	0.678	0.824	1.045	3.828	0.824
	SCN17	0.668	0.848	0.452	4.079	0.848
CHOW LINEAR	SCN11	0.535	0.711	-0.126	4.337	0.711
	SCN12	0.634	0.755	-0.003	3.940	0.755
	SCN13	0.711	0.793	0.084	3.579	0.793
	SCN14	0.772	0.826	0.152	3.248	0.826
	SCN15	0.942	0.943	0.377	1.784	0.943
	SCN16	0.950	0.976	0.532	1.574	0.976
	SCN17	0.807	0.886	0.657	3.369	0.886
HEC	SCN11	0.436	0.711	-0.210	4.606	0.711
(Combined	**SCN12**	**-5.390**	**0.019**	**-13.146**	**16.282**	**0.019**
standard and	SCN13	0.534	0.723	2.045	4.581	0.723
conservation	SCN14	0.357	0.692	-0.201	4.883	0.692
forms)	SCN15	0.814	0.884	-0.210	2.814	0.884
	SCN16	0.983	0.983	-0.213	0.946	0.983
	SCN17	0.885	0.912	-0.218	2.776	0.912
KINEROS	SCN11	0.487	0.818	-0.455	4.390	0.818
(θ=0.7)	SCN12	0.387	0.801	-1.088	4.624	0.801
	SCN13	0.207	0.764	-1.953	5.038	0.764
	SCN14	**N/S**	**N/S**	**N/S**	**N/S**	**N/S**
	SCN15	**N/S**	**N/S**	**N/S**	**N/S**	**N/S**
	SCN16	**N/S**	**N/S**	**N/S**	**N/S**	**N/S**
	SCN17	**N/S**	**N/S**	**N/S**	**N/S**	**N/S**

Note: RSQ - r squared; N/S - no solution.

It is interesting to see from Fig. 10 and Table 5 that the issue of odd solutions or large errors incurred by switching of equations for the HEC scheme does not improve but worsens by reducing the size of the temporal increment. And with the temporal increment shortening, the oscillation issue for the KINEROS scheme is not resolved either but becomes so worse that some of the scenarios have no solution. The magnitude of numerical dispersion for the Chow Linear scheme decreases when the temporal increment becomes shorter; however the variability of numerical dispersion for different sizes of the spatial increment is still very prominent. It also can be seen from Fig. 10 that the scheme

developed in this study has smaller variability of numerical dispersion for different scenarios than the Chow Linear scheme does, or the scheme is less dependent on the size of the spatial increment with respect to the magnitude of numerical dispersion. Table 5 also shows that the variability of the statistics of Ce, Cd and r squared for the scheme developed in this study is the smallest in comparison with those of the Chow Linear and HEC schemes even though some of the statistics are not as good as those of the Chow Linear and HEC schemes.

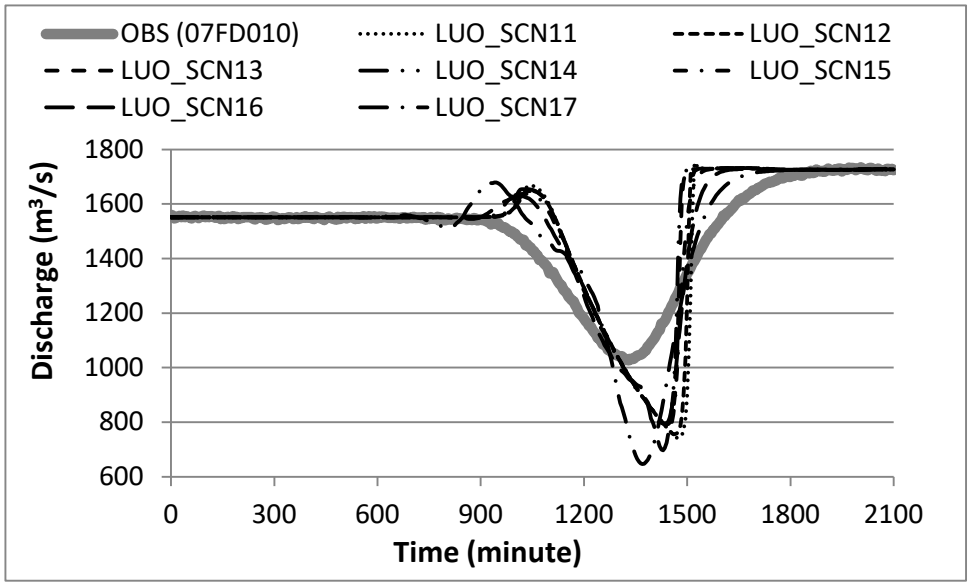

(a)

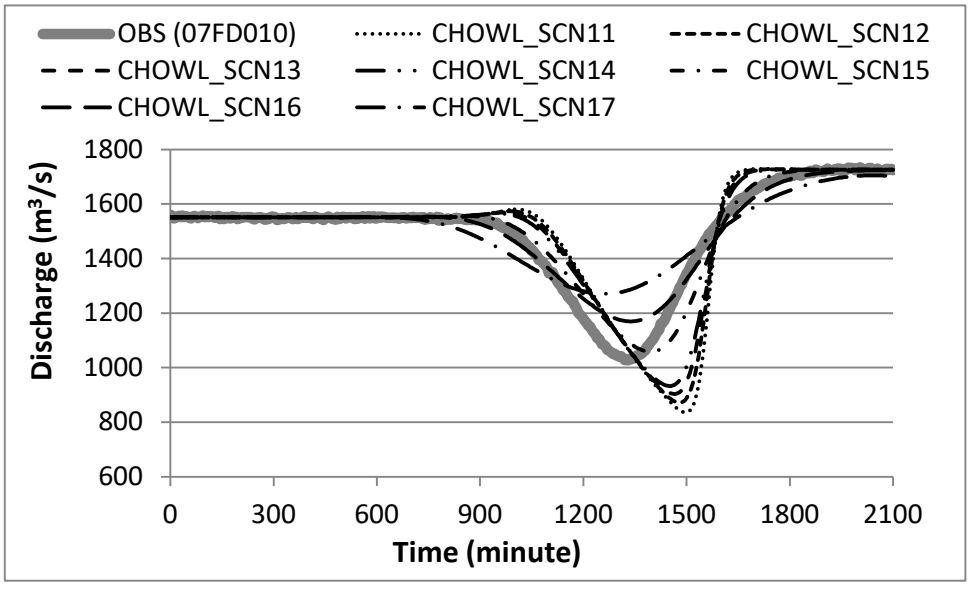

(b)

Figure 10. Comparison of simulated hydrographs from (a) scheme developed in this study (LUO), (b) Chow Linear scheme (CHOWL), (c) HEC scheme, and (d) KINEROS scheme (θ=0.7) with observed hydrograph for scenarios SCN11 to SCN17 (Δt = 5 minutes). (Continued next pages.)

(c)

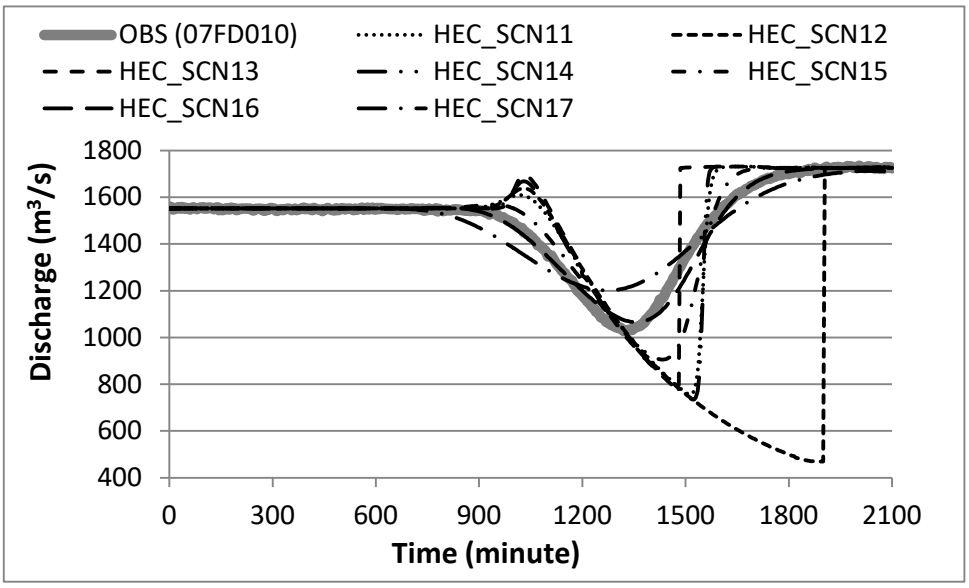

(d)

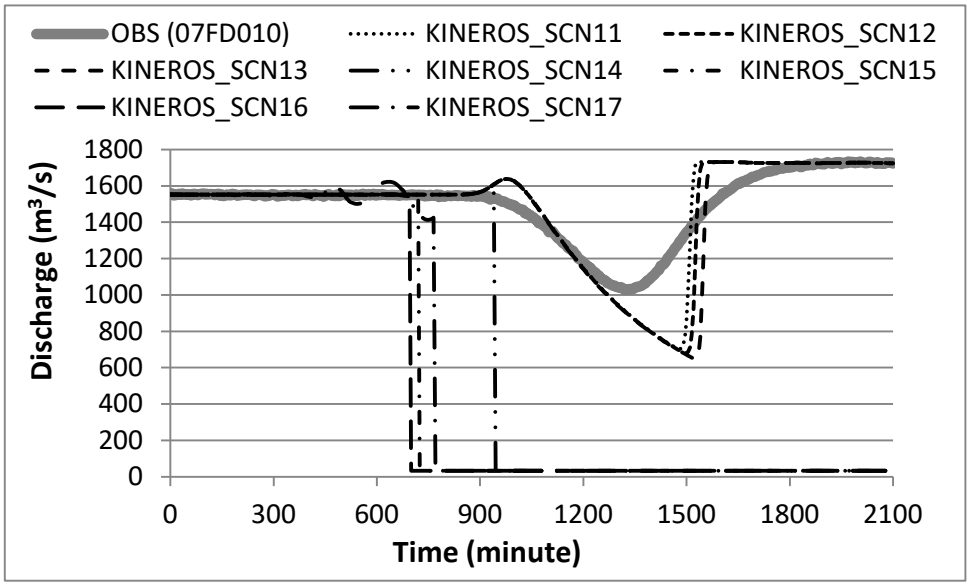

Figure 10. Comparison of simulated hydrographs from (a) scheme developed in this study (LUO), (b) Chow Linear scheme (CHOWL), (c) HEC scheme, and (d) KINEROS scheme (θ=0.7) with observed hydrograph for scenarios SCN11 to SCN17 (Δt = 5 minutes).

4.4 TVD test

In order to further determine whether the scheme developed in this study is TVD, a hypothetic rectangular inflow is employed to test the scheme for Scenarios SCN1 to SCN6 described in Subsections 3.3 and 4.2. All the channel parameters are the same as given in Subsection 3.3 and the Manning's rough coefficient (n) is the same as given in Subsection 4.2. Fig. 11 (a) shows the inflow and the outflows for the six scenarios, which are oscillation free. However, Fig.11 (b) shows clearly that there is a spurious

rising wedge in the outflow hydrograph at the turning point of the top of the rise for Scenario SCN1 (Δx = 1 km). A close look at this phenomenon reveals that this spurious rising wedge is actually incurred by oscillation at the most upstream spatial step.

(a)

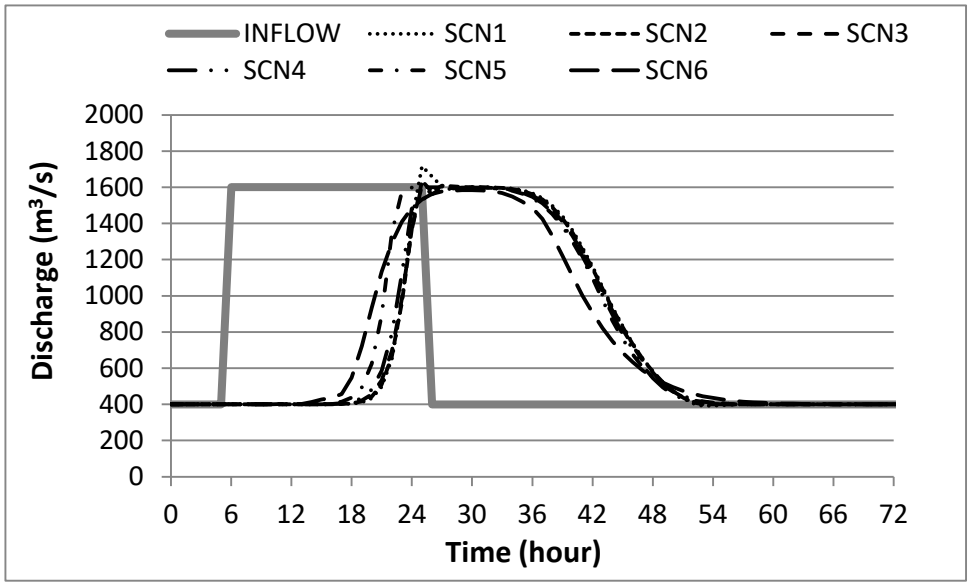

(b)

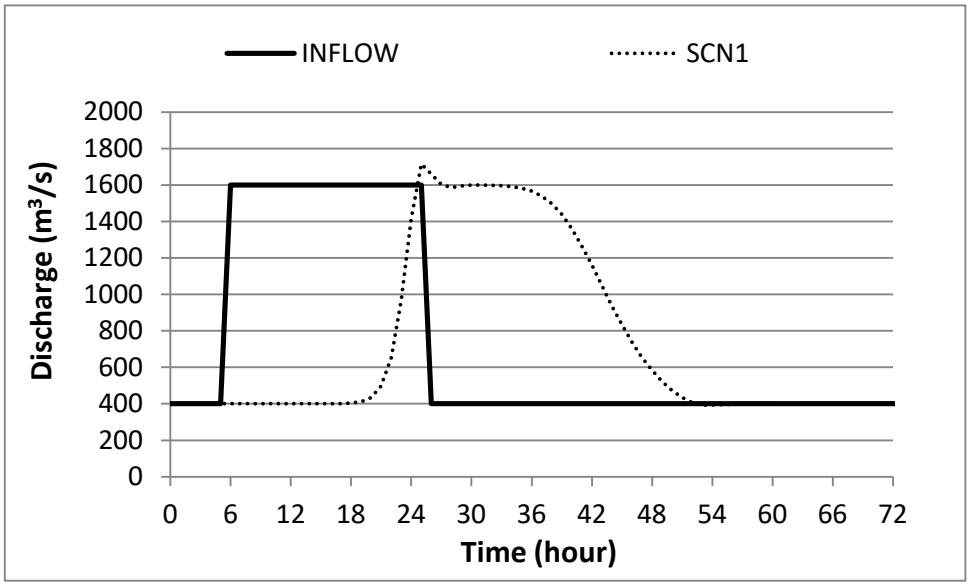

Figure 11. Rectangular inflow for TVD test and outflows for six scenarios: (a) Scenarios SCN1 to SCN6, and (b) Scenario SCN1 only.

Fig. 12 (a) shows the outflow hydrograph at the first spatial step next to the upstream boundary (x = Δx) and Fig. 12 (b) shows the outflow hydrograph at the tenth spatial step downstream of the upstream boundary (x = 10Δx). It can be seen clearly from Fig. 12 (a) that there is oscillation at the first

spatial step, but the oscillation diminishes rapidly downstream along the channel and the oscillation at the tenth spatial step, as shown in Fig. 12 (b), has lost most of its energy leaving the first wedge at position. The original definition of TVD (Harten, 1983; Sweby,1984) means that the total deviation at a time step is no greater than that at the previous time step. In this study, the flux limiter is defined on the temporal coordinate rather than on the spatial coordinate and therefore TVD means the total deviation at a downstream node is no greater than that at the upstream node, and in this regard the scheme developed in this study is a TVD scheme.

(a)

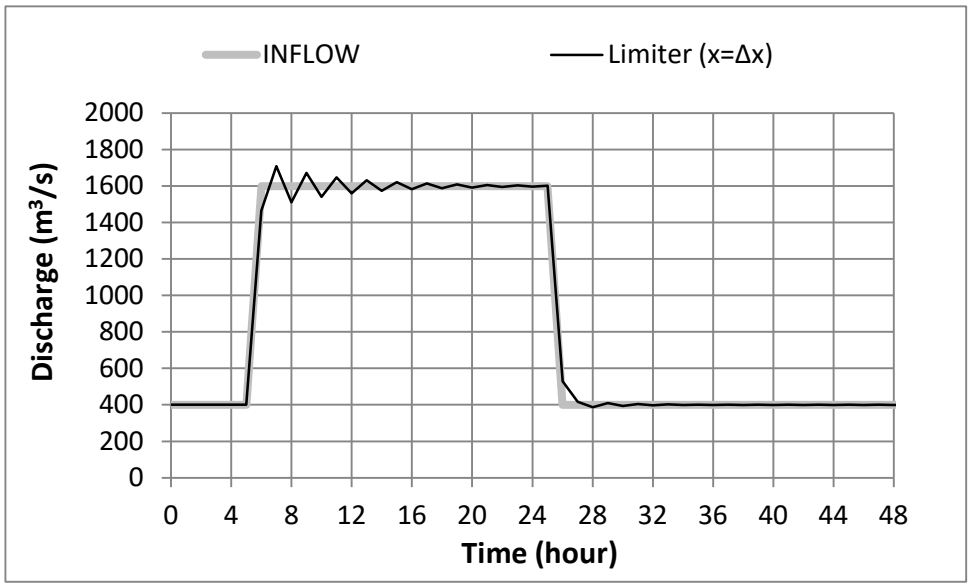

(b)

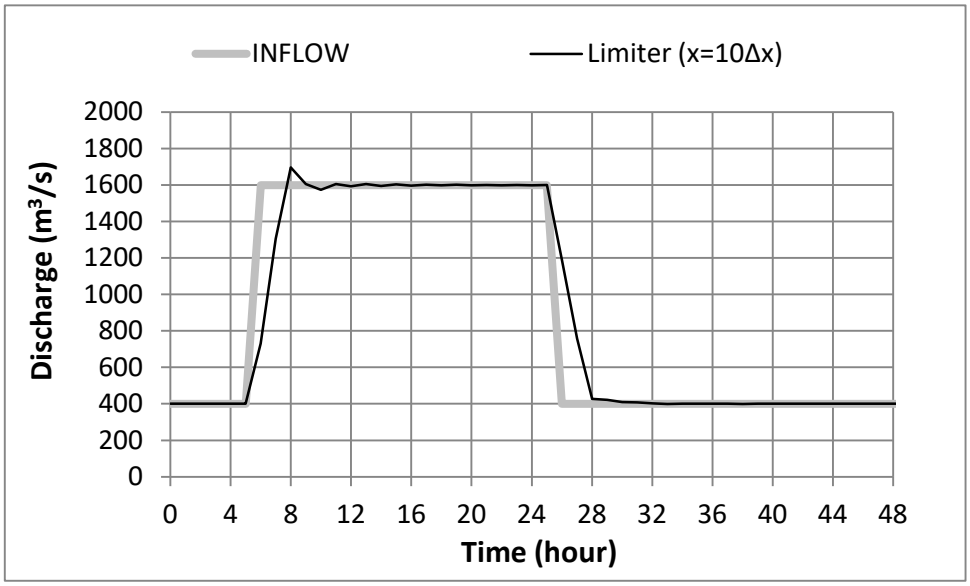

Figure 12. Outflow hydrographs for a rectangular inflow for Scenario SCN1, (a) x = Δx, and (b) x = 10 Δx (Δx = 1 km).

4.5 Routing the natural floods from snowmelt and coastal storms

In order to verify the ability of the scheme developed in this study in simulation of the natural floods in BC's watersheds, this scheme is utilized to simulate the two scenarios for the Fraser River near Marguerite (08MC018) and the Lillooet River near Pemberton (08MG005) in Section 3.2. Figs. 13 and 14 are the comparisons of the simulated hydrographs from the scheme developed in this study (LUO) and the outputs from the four commonly used schemes.

Figs. 13 and 14 shows that all the simulated hydrographs are very close to each other even though the simulated hydrograph from the scheme developed in this study has a 2 to 5 hours of time lags to those from the other schemes. These results demonstrate that, with certain efforts of calibration, the scheme developed in this study is equally accurate and efficient in simulation of the natural floods from the snowmelt and coastal storms.

(a)

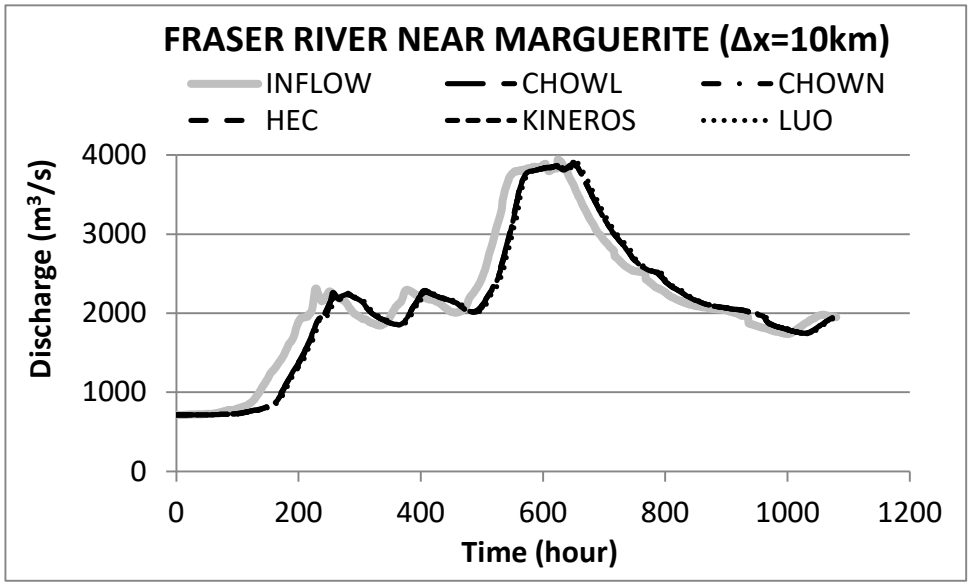

Figure 13. Comparison of output hydrographs for Scenario 1: [Δx = 10 km/ Δt = 1 h] and Scenario 2: [Δx = 20 km/ Δt = 1 h] for snowmelt flood inflow recorded at station Fraser River near Marguerite (08MC018). LUO represents this study, CHOWL represents Chow Linear and CHOWN represents Chow Nonlinear. (a) Complete hydrograph for Scenario 1, (b) peaking part for Scenario 1, (c) complete hydrograph for Scenario 2, and (d) peaking part for Scenario 2. (Continued next pages.)

(b)

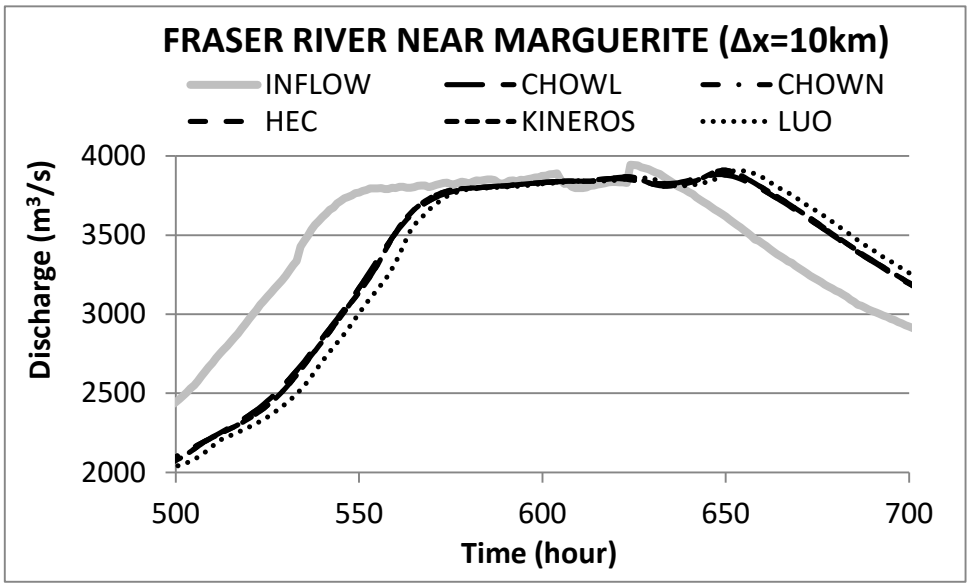

(c)

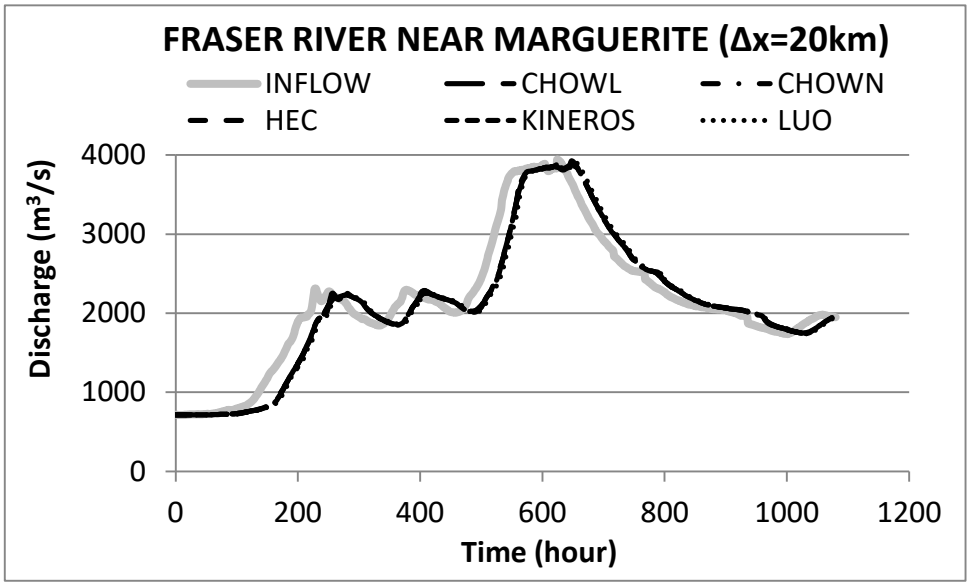

Figure 13. Comparison of output hydrographs for Scenario 1: [Δx = 10 km/ Δt = 1 h] and Scenario 2: [Δx = 20 km/ Δt = 1 h] for snowmelt flood inflow recorded at station Fraser River near Marguerite (08MC018). LUO represents this study, CHOWL represents Chow Linear and CHOWN represents Chow Nonlinear. (a) Complete hydrograph for Scenario 1, (b) peaking part for Scenario 1, (c) complete hydrograph for Scenario 2, and (d) peaking part for Scenario 2. (Continued next page.)

(d)

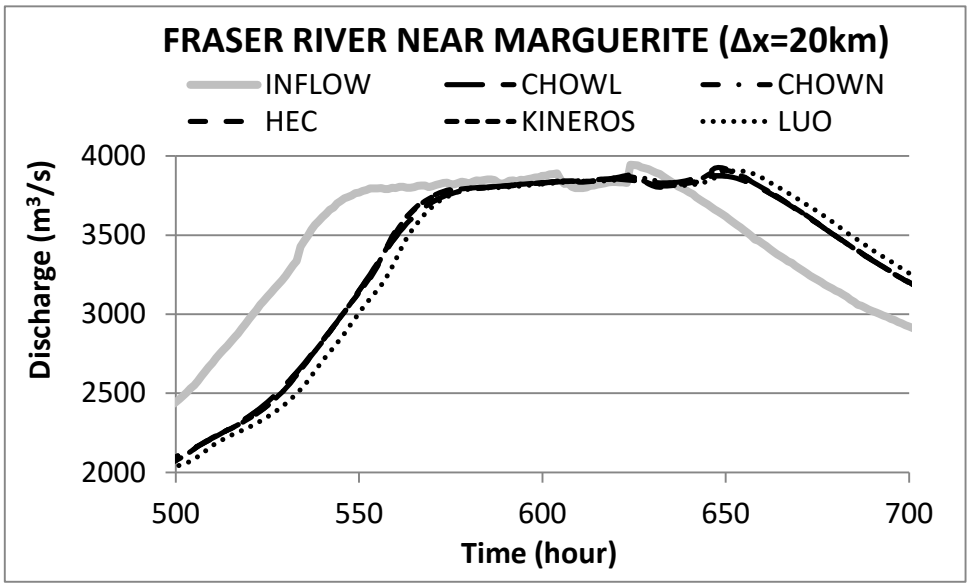

Figure 13. Comparison of output hydrographs for Scenario 1: [Δx = 10 km/ Δt = 1 h] and Scenario 2: [Δx = 20 km/ Δt = 1 h] for snowmelt flood inflow recorded at station Fraser River near Marguerite (08MC018). LUO represents this study, CHOWL represents Chow Linear and CHOWN represents Chow Nonlinear. (a) Complete hydrograph for Scenario 1, (b) peaking part for Scenario 1, (c) complete hydrograph for Scenario 2, and (d) peaking part for Scenario 2.

(a)

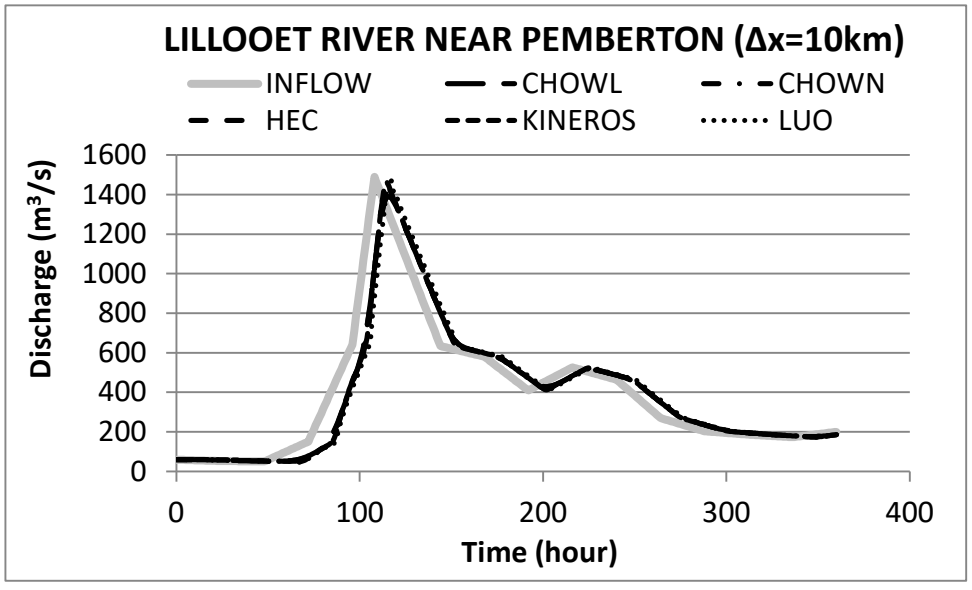

Figure 14. Comparison of output hydrographs for Scenario 1: [Δx = 10 km/ Δt = 1 h] and Scenario 2: [Δx = 20 km/ Δt = 1 h] for coastal storm flood inflow recorded at station Lillooet River near Pemberton (08MG005). (Continued next pages.)

(b)

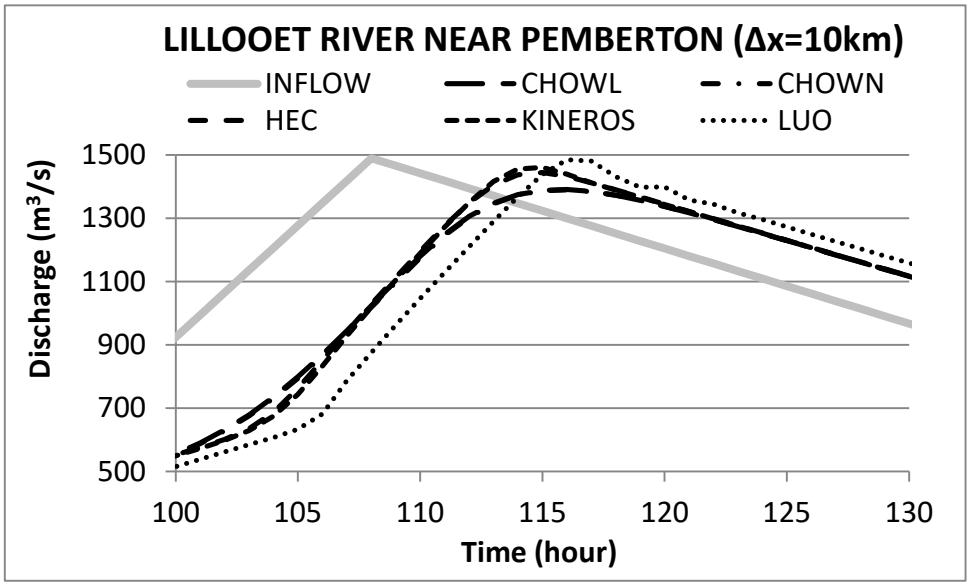

(c)

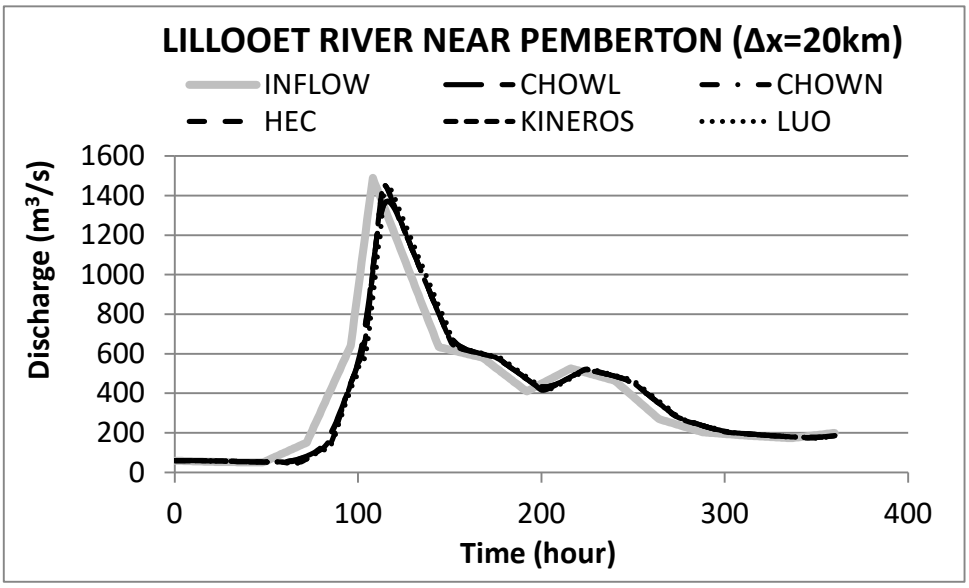

Figure 14. Comparison of output hydrographs for Scenario 1: [Δx = 10 km/ Δt = 1 h] and Scenario 2: [Δx = 20 km/ Δt = 1 h] for coastal storm flood inflow recorded at station Lillooet River near Pemberton (08MG005). LUO represent this study, CHOWL represents Chow Linear and CHOWN represents Chow Nonlinear. (a) Complete hydrograph for Scenario 1, (b) peaking part for Scenario 1, (c) complete hydrograph for Scenario 2, and (d) peaking part for Scenario 2. (Continued next page.)

(d)

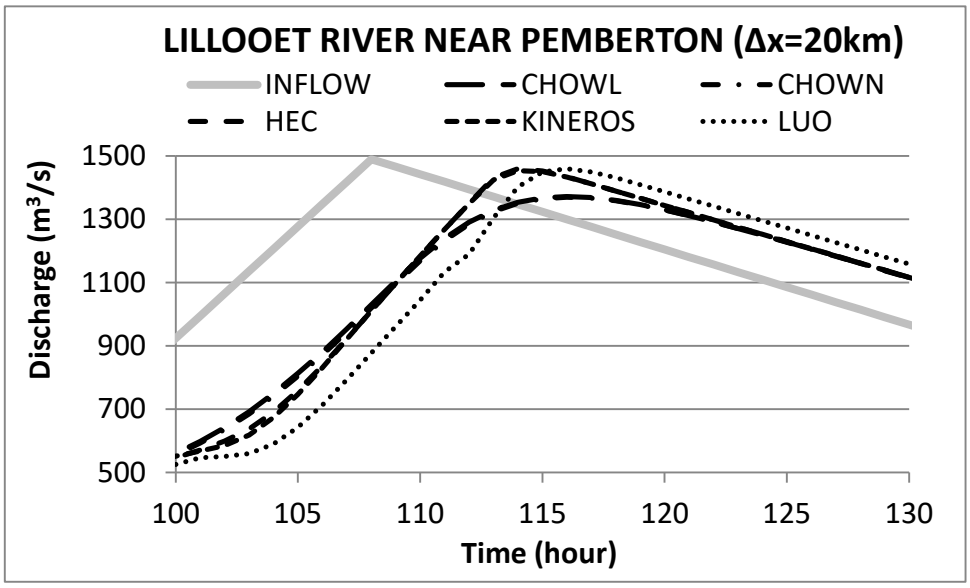

Figure 14. Comparison of output hydrographs for Scenario 1: [Δx = 10 km/ Δt = 1 h] and Scenario 2: [Δx = 20 km/ Δt = 1 h] for coastal storm flood inflow recorded at station Lillooet River near Pemberton (08MG005). LUO represent this study, CHOWL represents Chow Linear and CHOWN represents Chow Nonlinear. (a) Complete hydrograph for Scenario 1, (b) peaking part for Scenario 1, (c) complete hydrograph for Scenario 2, and (d) peaking part for Scenario 2.

4.6 Comparison with Muskingum-Cunge

There are a number of variants of the Muskingum-Cunge (MC) approach and discussion of these variants is beyond the scope of this paper and can be found in Todini (2007). However, the basic form of MC from Chow et al. (1988) and US Army Corps of Engineers (1991) is used to simulate the regulated inflow for the seven scenarios defined in Section 3.3 and Table 1. Fig. 15 is the comparison of the simulated hydrographs from MC with the observed hydrograph. One can see from Fig. 5 that oscillation is present at the peaks for SCN7. This implies that MC is actually of second order accuracy and thus is not TVD. Table 6 is the statistics of the simulated hydrographs for the sever scenarios. It is interesting to see from Table 6 that the performance of MC for the scenarios with smaller spatial increments (SCN1 to SCN3) is not as good as for those of larger spatial increments (SCN4 and SCN6) except for SCN7. Comparing Table 6 and Table 3, it can be seen that the performance of the scheme developed in this study for SCN1 to SCN3 is better than that of MC. Even though MC for SCN4 to SCN6 performs better than the scheme developed in this study, MC incurs oscillation for SCN7 and therefore is not preferable for the open channel routing for the regulated inflow.

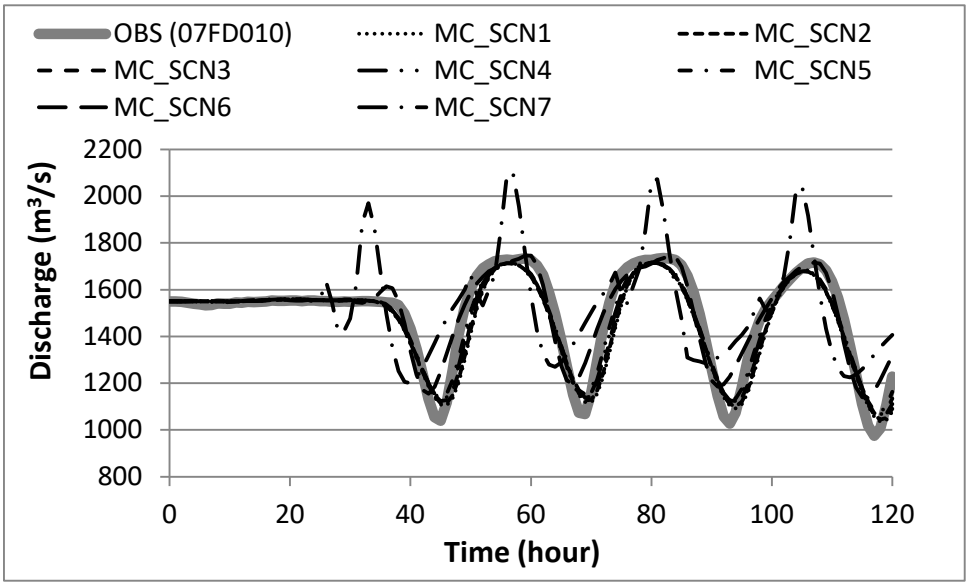

Figure 15. Comparison of simulated hydrographs from Muskingum-Cunge (MC) approach with observed hydrograph for Scenarios SCN1 to SCN7.

Table 6. Statistics of simulated hydrographs from Muskingum-Cunge (MC) approach for SCN1 to SCN7 (Δt = 1 hour = 3600 s).

Scheme	Scenario	Ce	Cd	dV (%)	Era (%)	RSQ
MC	SCN1	0.87	0.897	-2.321	3.505	0.897
	SCN2	0.883	0.906	-2.063	3.367	0.906
	SCN3	0.904	0.922	-1.655	3.129	0.922
	SCN4	0.923	0.938	-1.274	2.871	0.938
	SCN5	0.939	0.954	-0.902	2.591	0.954
	SCN6	0.871	0.892	1.047	3.155	0.892
	SCN7	0.111	0.335	2.934	10.041	0.335

Note: RSQ - r squared.

5. Conclusions

Starting with examination of the four commonly used numerical schemes, Chow Linear and Nonlinear, HEC and KINEROS, for the kinematic wave open channel routing with the example from Chow et al. (1988) and three typical observed hydrographs from the large-scale watersheds in BC as the inflows, this paper developed a high resolution numerical scheme for the kinematic wave open channel routing in order to overcome the difficulties faced by the four commonly used schemes. The scheme developed in this study is stable after introducing the flux limiter Minmod (Roe, 1981; 1986) to the equation and is

less grid-size (of spatial and temporal increments) dependent in comparison with the Chow Linear and Nonlinear schemes. The equations of this scheme are solved iteratively by employing a method similar to the SIMPLE. When examined with the regulated hydrograph recorded at the WSC station located on the Peace River in BC, Canada as the inflow for two sizes of the temporal increment (1 hour and 5 minutes) and seven sizes of the spatial increment so that the quotient of $\Delta x/\Delta t$ covers the minimum and maximum kinematic wave celerities, this scheme does not exhibits oscillation as the KINEROS scheme (and the MC as well) does or has the issue of odd solutions (large errors) incurred by switching of equations as the HEC scheme does. This stable and less grid-size dependent high-resolution scheme gives a modeller more flexibility in selection of the sizes of the spatial and temporal increments. It can be concluded that this scheme is more appropriate and efficient for the kinematic wave open channel routing for the large-scale watershed modeling in BC.

References

Alfieri, L., Burek, P., Dutra, E., Krzeminski, B., Muraro, D., Thielen, J., Pappenberger, F., 2013. GloFAS – global ensemble streamflow forecasting and flood early warning. Hydrol. Earth Syst. Sci., 17, 1161–1175.

Burek, P., van der Knijff, J., de Roo, A., 2013. LISFLOOD: Distributed Water Balance and Flood Simulation Model, Revised User Manual, JRC78917, EUR 26162 EN, Luxembourg: Publications Office of the European Union, 2013. http://ies.jrc.ec.europa.eu/the-institute/units/water-resources.html.

Chakravarthyan, S., Osher, S. 1983. High resolution applications of the Osher upwind scheme for the Euler equations, AIAA paper presented at 6th CFD conference 1983.

Chow, V.T., Maidment, D.R., Mays, L.W.,1988. Applied Hydrology. McGraw-Hill, New York.

Dawdy, D., 1990. Discussion of “Kinematic wave routing and computational error” by T. V. Hromadka II and J. J. DeVries (February, 1988, Vol. 114, No. 2)." J. Hydraul. Eng., 10.1061/(ASCE)0733-9429(1990)116:2(278), 278-280.

Demargne, J., Wu, L., Regonda, S., Brown, J., Lee, H., He, M., Seo, D.-J., Hartman, R., Herr, H., Fresch, M., Schaake, J., Zhu, Y., 2014. The science of NOAA’s operational hydrologic ensemble forecast service. Bull. Am. Meteorol. Soc., http://dx.doi.org/10.1175/BAMS-D-12-00081.1.

De Roo, A., 1999. LISFLOOD: a rainfall-runoff model for large river basins to assess the influence of land use changes on flood risk, in Balabanis, P. (ed.),: Ribamod: River Basin Modelling, Management and Flood Mitigation, Concerted action, European Commission, EUR 18287 EN, 349–357, 1999.

Goodrich, D.C., 1992. Discussion of “The kinematic wave controversy” by Victor M. Ponce (April, 1991, Vol. 117, No. 4)." J. Hydraul. Eng., 10.1061/(ASCE)0733-9429(1992)118:9(1334), 1334-1335.

Harten, A., 1983. High resolution Schemes for hyperbolic conservation laws. J. Comp. Phys. 49 (3), 357-393.

Hromadka, T.V., DeVries, J.J., 1988. Kinematic Wave Routing and Computational Error. J. Hydraul. Eng.,

ASCE 114(2), 207-217.

Koren, V., Reed, S., Smith, M., Zhang, Z., Seo, D.-J., 2004. Hydrology Laboratory Research Modeling System (HL-RMS) of the National Weather Service. Journal of Hydrology, 291, 297–318.

Lee, K.T., Huang, P.C., 2012. Evaluating the adequateness of kinematic-wave routing for flood forecasting in midstream channel reaches of Taiwan. Journal of Hydroinformatics 14(4), 1075-1088. DOI: 10.2166/hydro.2012.093.

Lettenmaier, D.P., Wood, E.F., 1992. Chapter 26 Hydrologic forecasting, in: Maidment, D.R. (Ed.), Handbook of Hydrology, McGraw-Hill Inc., pp. 26.1-26.30.

Lien, F.S., Leschziner, M.A, 1994. Upstream monotonic interpolation for scalar transport with application to complex turbulent flows. Int. J. Num. Meth. Fluids 19 (6), 527–548.

Luo, C., 2015. Technical Reference for The CLEVER Model – A Real-time Flood Forecasting Model for British Columbia, Technical Report, BC River Forecast Centre.

Luo, C., Gardner, T., Campbell, D., 2015. Evaluation of the CLEVER Model – a real-time flood forecast model for large-scale watersheds in British Columbia, Proceedings of CWRA BC Branch Conference, Vancouver, BC, Canada, 18-25 November, 2015.

Luo, Q., 2007. A distributed surface flow model for watersheds with large water bodies and channel loops. Journal of Hydrology 337, 172–186.

McEnery, J., Ingram, J., Duan, Q., Adams, T., Anderson, L., 2005. NOAA'S Advanced Hydrologic Prediction Service: Building pathways for better science in water forecasting. Bulletin of the American Meteorological Society, 86 (3), 375-385.

Meselhe, E.A., Holly, F.M., 1997. Invalidity of Preissmann scheme for transcritical flow. J. Hydraulic Eng. 123 (7), 652-655.

Moramarco, T., Singh, V. P., 2000. A practical method for analysis of river waves and for kinematic wave routing in natural channel networks. Hydrological Processes 14, 51-62.

Nash, J.E., J.V. Sutcliffe, 1970. River flow forecasting through conceptual models, 1. A discussion of principles. Journal of Hydrology 10, 282-290.

Patankar, S.V., Spalding, D.B., 1972. A calculation procedure for heat, mass and momentum transfer in three-dimensional parabolic flows. International Journal of Heat Mass Transaction 15, 1787–1806.

Ponce, V.M., 1991. Kinematic wave controversy. J. Hydraul. Eng., 10.1061/(ASCE)0733-9429(1991)117:4(511), 511-525.

Ponce, V.M., 1996. Modeling surface runoff with kinematic, diffusion, and dynamic waves, in: Singh, V.P., Kumar, B. (Ed.), Proceedings of the International Conference on Hydrology and Water Resources, New Delhi, India, December 1993, Volume 1, Surface-Water Hydrology, Springer Scinece+Nusiness Media, B.V., pp. 121-132.

Preissmann, A., 1961. Propagation des intumescences dans les canaux et Rivieres. First Congr. des l'Assoc. Francaise de Calcul, Association Francaise de Calcul, Grenoble, France, 433-422.

Roe, P.L., 1981. Approximate Riemann solvers, parameter vectors, and difference schemes. J. Comp. Phys., 43, 357-372.

Roe, P.L., 1986. Characteristic-based schemes for the Euler equations, Ann. Rev. Fluid Mech. 18, 337–365.

Singh, V.P., 1996. Kinematic Wave Modeling in Water Resources: Surface-Water Hydrology, John Wiley & Sons, New York.

Smith, R.E., Goodrich, D.C., Woolhiser, D.A., Unkrich, C.L., 1995; 2012. Chapter 20, KINEROS - A KINematic Runoff and EROSion Model, in: Singh, V.P. (Ed.), Computer Models of Watershed Hydrology. Water Resources Publications, pp. 697-732.

Sweby, P. K., 1984. High resolution schemes using flux limiters for hyperbolic conservation laws. SIAM Journal on Numerical Analysis, 21(5), 995-1011.

Syed, A.U., Nejadhashemi, A.P., Safferman, S., Lusch, D. , Bartholic, J., Segerlind, L.J., 2012. A comparative analysis of kinematic wave and SCS-unit hydrograph models in semi-arid watershed. XIX International Conference on Water Resources CMWR 2012, University of Illinois at Urbana-Champaign, June 17-22, 2012.

Thielen, J., Bartholmes J., Ramos, M.-H., de Roo, A., 2009. The European Flood Alert System – Part 1: Concept and development. Hydrol. Earth Syst. Sci., 13, 125–140.

Thiemig, V., Bisselink, B., Pappenberger, F., Thielen ,J., 2015. A pan-African medium-range ensemble flood forecast system. Hydrol. Earth Syst. Sci., 19, 3365–3385.

Todini, E., 2007. A mass conservative and water storage consistent variable parameter Muskingum-Cunge approach. Hydrol. Earth Syst. Sci., 11, 1645–1659.

US Army Corps of Engineers, 1991. A Muskingum-Cunge Channel Flow Routing Method for Drainage Networks, TP-135, Institute for Water Resources, Hydrologic Engineering Centre, http://www.hec.usace.army.mil/publications/TechnicalPapers/TP-135.pdf. (last access: August 10, 2016).

US Army Corps of Engineers, 1993. Introduction and Application of Kinematic Wave Routing Techniques Using HEC-1, TD-10. Institute for Water Resources, Hydrologic Engineering Centre, http://www.hec.usace.army.mil/publications/TrainingDocuments/TD-10.pdf, (last access: August 10, 2016).

US Army Corps of Engineers, 2000. Hydrologic Modeling System HEC-HMS, Technical Reference Manual, March 2000, CPD-74B. Institute for Water Resources, Hydrologic Engineering Centre, http://www.hec.usace.army.mil/software/hec-hms/documentation/HEC-HMS_Technical%20Reference%20Manual_(CPD-74B).pdf, (last access: last access: August 10, 2016).

Van Albada, G.D., Van Leer, B., Roberts, W.W., 1982. A comparative study of computational methods in cosmic gas dynamics. Astronomy and Astrophysics, 108, 76–84.

Van Leer, B., 1974. Towards the ultimate conservative difference scheme, 11. Monotonicity and

conservation combined in a second order scheme. J. Comp. Phys., 14, 361-370.

Van Leer, B. 1977. Towards the ultimate conservative difference scheme III. Upstream-centered finite difference schemes for ideal compressible flow. J. Comp. Phys. 23 (3): 263–275.

Waterson, N.P., Deconinck, H., 1995. A unified approach to the design and application of bounded higher-order convection schemes. In: Taylor, Durbetaki (Eds.), Proceedings of the Ninth International Conference on Numerical Methods in Laminar and Turbulent Flow, Atlanta, July, 1995. Pineridge Press, Swansea.

Ye, A., Duan, Q., Zhan, C., Liu, Z., Mao, Y., 2013. Improving kinematic wave routing scheme in Community Land Model. Hydrology Research 44.5, 886-903. DOI: 10.2166/nh.2012.145.

Yu, C., Duan, J.G., 2014. High resolution numerical schemes for solving kinematic wave Equation. Journal of Hydrology 519, 823–832.